Studies on the role of CheS in *Sinorhizobium meliloti* chemotaxis

Gaurav Dogra

Thesis submitted to the faculty of the Virginia Polytechnic Institute and State University in partial fulfillment of the requirements for the degree of

Master of Science
in
Biological Sciences

Birgit E. Scharf, Chair
Timothy J. Larson
David L. Popham
Florian D. Schubot

August 1st, 2011

Blacksburg, VA

Keywords: flagellar motor, phosphatase, phosphorylation, two-component system

Studies on the role of CheS in *Sinorhizobium meliloti* chemotaxis

Gaurav Dogra

Biological Sciences
Virginia Tech

Abstract

Chemotaxis is the ability of an organism to sense its environment and move towards attractants and away from repellents. The two-component system controlling chemotaxis in bacteria contains a histidine kinase CheA, which is autophosphorylated in response to a signal from a ligand-bound transmembrane methyl-accepting chemotaxis protein. CheA transfers the phosphate group to its cognate response regulator which modulates flagellar rotation. Signal termination by dephosphorylation of the response regulator is necessary for the organism to react rapidly to changes in the environment. The phosphorylated response regulator CheY in *Escherichia coli* is dephosphorylated by CheZ, a phosphatase; certain organisms, such as *Sinorhizobium meliloti*, that lack a CheZ homolog have developed alternate methods of signal termination. The signaling chain of *S. meliloti* contains two response regulators, CheY1 and CheY2, in which CheY2 modulates flagellar rotation and CheY1 causes signal termination by acting as a phosphate sink. In addition to known chemotaxis components, the second gene in the chemotaxis operon of *S. meliloti* codes a 97 amino acid protein, called CheS. The phenotype of a *cheS* deletion strain is similar to that of a *cheY1* deletion strain. Therefore, the possibility that CheS causes signal termination was explored in this work. The derived amino acid sequence of CheS showed similarities with its orthologs from other α-proteobacteria. Sequence conservation was highest at the centrally located α4 and α5 helices. Earlier observations that CheS localizes at the polar chemotaxis cluster in a CheA-dependent manner were confirmed. The co-

localization of CheS with CheA was demonstrated by fluorescence microscopy. The stable expression of CheS in the presence of CheA was confirmed by immunoblot. The same approach was used to establish the stable expression of CheS only in the presence of the P2 domain of CheA, but not with the P1 or P345 domains. Limited proteolysis followed by mass spectrometry defined $CheA_{163-256}$ as the CheS binding domain, and this domain overlapped the previously defined CheY2-binding domain, $CheA_{174-316}$. The role of CheS in the phosphate flux in *S. meliloti* chemotaxis was analyzed by assays using radio-labeled [γ-^{32}P]ATP. CheS does not play a role in the autophosphorylation of CheA. However, CheS accelerated the rate of CheY1~P dephosphorylation by almost two-fold, but did not affect the rate of CheY2~P dephosphorylation. CheS also does not seem to affect phosphate flow in the retrophosphorylation from CheY2~P to CheA using acetyl [^{32}P]phosphate as phosphodonor. Since CheS increases the rate of CheY1 dephosphorylation, it can be envisioned that it either increases the association of CheY1 to CheA, increasing the flow of phosphate from CheA to CheY1, or directly accelerates the dephosphorylation of CheY1~P. The presence of a STAS domain and a conserved serine residue in CheS also raises the possibility that CheS may be phosphorylated by a yet unknown kinase, in a mechanism similar to the phosphorylation of *Bacillus subtilis* SpoIIAA by its cognate kinase SpoIIAB. Phosphorylated CheS may then switch CheA between a kinase or phosphotransferase ON/OFF state or activated CheS may directly interact with CheY1. Further studies are needed to determine the association of CheY1 with CheS to elucidate the mechanism of CheY1 dephosphorylation. This work has confirmed the *in vitro* association of CheS with CheA, determined the CheS binding domain on CheA, and indicated that CheS accelerates the dephosphorylation of CheY1~P. This has advanced our understanding of the role of CheS in the chemotaxis signaling chain of *S. meliloti.*

Dedication

First and foremost, my deepest gratitude and thanks are due to my advisor, Dr. Birgit Scharf, for her unequivocal guidance, affection and genuine concern for my academic and emotional well-being. I would not have succeeded in achieving my objectives had it not been for her tireless dedication to her craft and her genuine affection for her students and selflessness, which she had shown to me throughout my tenure with her. She is indeed an inspiration and a fitting example of a great professor, and that of a kind, genuine human being. I would also like to extend my gratitude to my committee members, Drs. Timothy Larson, David Popham and Florian Schubot who were kind and patient, and always provided valuable input to my research.

Thanks are due to Frauke Purschke and Verena Wagner for earlier work, and for taking the project off the ground. I would also like to thank our collaborators, Drs. Richard Helm and Keith Ray for their patient work on determining amino acid sequence of the CheS binding domain using MS/MS analysis. Their expertise and assistance helped us complete a very significant portion of the project.

Critical to any work environment are good colleagues. I was blessed to have a wonderful lab environment and some of the best colleagues I could have asked for. Special thanks are due to Hardik Zatakia for being a good support structure and for being a great friend. Thanks are also due to Ben Webb whose jollity was infectious, and to Crystal Gilbert, our ultra-efficient lab tech who was always patient and kind towards me. I would like to acknowledge Jonathan Hughes, who was a research associate in the Scharf Lab before I joined the team, and was responsible for creating some of the *S. meliloti* strains I used in my studies. I appreciate the wonderful enthusiasm of my undergraduate colleagues, especially Melanie Niemeyer, who I mentored in the fall of 2010. Her willingness to learn, positive attitude and our “finer things club” coffee time will be fondly remembered.

Finally, I would like to thank God, family and friends for their undying support and love, which enabled me to sail through any situation, good, bad or worse, and for their patience and understanding in situations where I might not have been equally understanding or patient. My parents have always been my strength and my guiding principle. I owe my education to their undying efforts. I would also like to acknowledge Lyndon Judge, who has made the most significant impact on my life, and made me feel loved. Her support and affection through this time of my life and her undying encouragement are both uplifting and moving. Our little dog Lambo is a source of great entertainment, except when he ate all my Baby Ruths. He is ‘man’s best friend’ indeed.

Table of Contents

List of Figures

List of Tables

Chapter 1

Introduction

Modes of bacterial swimming motility

Chemotaxis is the ability of a microorganism to move towards favorable environmental conditions such as adequate food and pH. The first observation of bacterial motility came from Antony Van Leeuwenhoek's studies in 1676. The bacterial flagellum was first described by Ehrenberg in 1838 (17). The capillary method to measure chemotaxis was developed by Wilhelm Pfeffer in 1883 (59). No significant advances in studies of chemotaxis were made until Julius Adler's ground-breaking work in the 1960s (1, 49). In a series of seminal papers, Adler described the mechanisms of chemoeffector sensing by methyl accepting chemotaxis proteins (MCPs) of the γ-proteobacterium *Escherichia coli* which relayed environmental cues via an intracellular signal transduction chain to the flagellar motor (34, 35). Silverman and Simon developed genetic approaches in the 1970s that established links between *che* genes and Che proteins (78, 79).

The movement of an *E. coli* cell alternates between phases of smooth swimming (runs) and short reorientations (tumbles), described as the 'random walk' (9). *E. coli* has an average of six to eight flagella (Figure 1.1) which are driven by a rotary motor at the base. Counter-clockwise (CCW) rotation of the flagella results in smooth swimming due to the formation of a bundle which serves to propel the bacterium in a run. A change in rotation of any of these flagella in the opposite direction, clockwise (CW), results in the disruption of the bundle and tumbling motility, where the cell moves randomly over very short distances (18, 19). The conversion of the random walk in to a more focused movement towards a chemoattractant is the central theme of chemotaxis and is called the 'biased random walk' (9). In the absence of a chemoattractant or the presence of a chemorepellent, the MCP initiates a chemotactic signal chain to the flagellar motor which results in an increased

tumble rate and reorients the cell towards attractants and away from repellents. The net effect of this synchronized run and tumble is the ability of the bacterium to swim up an attractant gradient or down a repellent gradient. Due to the small size of the bacterial cell, sensing of chemoeffector gradients is temporal (10, 15, 42).

The flagellar motor of *Escherichia coli*

The flagellar apparatus can be divided into three main parts: a rigid filament, a short, flexible hook structure and a basal body (Figure 1.2). The bacterial flagellar filament consists of 11 protofilaments of tens of thousands of subunits of a protein called FliC (flagellin) arranged in a helical fashion (69). Filaments are up to 15μm long and 25 nm in diameter. A switch from CCW to CW rotation induces a helical transition in the filament from left- to right-handedness. Concomitantly, the right-handed helix transforms to semi-coiled and curly which allows it to disassociate from other left-handed flagella rotating in the CCW direction to form a bundle (32, 43, 98).

The hook structure is a flexible polymer formed by FlgE that forms a twisted tubular structure 55 nm long with a 25 nm channel in the center (51, 70, 99). It transfers the torque generated by the basal body to the flagellar filament and thus acts as a universal flexible hinge. The basal body is composed of several rings mounted on a central rotating rod and are named according to their location: L-ring for *l*ipopolysaccharide, P-ring for *p*eptidoglycan, S-*s*upramembrane and M-*m*embrane form the MS ring, and C-ring for *c*ytoplasm. The L and P rings do not rotate and form bearings to support the rod. The transmembrane stator proteins MotA and MotB form torque-generating units surrounding the rotating part of the motor. The electrostatic interactions between MotA and the C-ring protein FliG result in flagellar rotation (40, 85).

Regulation of chemotaxis in *E. coli*

Two component signal transduction systems consist of receptor/s, a central histidine autokinase and a cognate response regulator (53). In bacterial chemotaxis, the response regulator interacts with FliM at the flagellar C-ring and causes a tumble reaction. *E. coli* has five chemoreceptors, which include four methyl-accepting chemotaxis proteins (MCPs) and an aerotaxis transducer (Aer) (76) that enable the detection of a wide variety of environmental cues including amino acids, sugars, dipeptides, pH, and oxygen tension. Arranged at the cell poles, the MCPs are connected to the histidine autokinase CheA through an adapter protein CheW (13, 68). The histidine autokinase CheA forms a dimer with a conserved His-48 residue responsible for phosphotransfer on each monomer (90).

An MCP consists of a periplasmic sensing domain, a transmembrane domain and a cytoplasmic signaling domain. In the presence of a chemorepellent, a piston-like movement of the transmembrane helices causes a change in the signaling domain and activates the kinase activity of CheA to cause intramolecular cross phosphorylation of the His-48 residues by each CheA monomer (54). The phosphate group from CheA~P is then transferred to the cognate response regulator, CheY at the Asp-57 residue (14, 28). The phosphorylated CheY~P binds to the flagellar motor protein FliM causing a switch from CCW to CW rotation (37). When one or more of the flagella switch rotation from CCW to CW, the flagellar propulsive bundle breaks up, and the cell starts tumbling. The tumbling behavior is determined by the intracellular CheY~P concentration (37, 73). A very important player in the regulation of CheY~P levels is the phosphatase CheZ (89), which removes the phosphate group from CheY~P and accelerates dephosphorylation about 10-

fold more than the intrinsic rate of autodephosphorylation of CheY (27, 80, 81) (Figure 1.3).

However, in the presence of a constant concentration of attractant or repellent, a bacterium needs the ability to reset its chemotactic sensory mechanism. This ability is called adaptation (33). The sensitivity of a chemoreceptor is determined by its methylation level which is controlled by the proteins CheB and CheR. CheR is a methyltransferase that covalently modifies conserved 4-6 glutamate residues on the cytoplasmic surface of each MCP resulting in a reduced affinity of the ligand-binding domain to its substrate (3). CheB is a methylesterase response regulator that hydrolyzes the methyl esters and decreases the methylation state of the receptor thereby increasing the sensitivity of the sensing domain (87). CheB is activated through phosphorylation by CheA (41).

Sinorhizobium meliloti is a plant symbiont

Increasing interest in the chemotaxis signaling chain of non-enteric bacteria in recent years has led to new insights into structures and molecular mechanisms that differ from the enterobacterial paradigm (6, 74). Members of the α-subgroup of proteobacteria such as *Agrobacterium*, *Rhizobium, Caulobacter*, *Rhodobacter,* and *Sinorhizobium,* depart from the enteric chemosensory pathway.

Sinorhizobium meliloti forms a symbiotic relationship with the plants *Medicago sativa* (alfalfa) and *Medicago truncatula* (barrel medic) and *Melilotus alba* (white sweet clover) (7, 24, 31). A complex chain of signal exchanges between the plant and *S. meliloti* allow the bacterium to invade roots. Plant-secreted flavonoids bind to *S. meliloti* NodD proteins resulting in their activation (58). NodD proteins bind to specific promoters on the bacterial genome resulting in the production of lipopolysaccharides called Nod (for *Nod*ulation)

factors (56). A combination of Nod factors and exopolysaccharides cause root hair curling followed by the formation of structures called infection threads (97). The internalized bacteria differentiate into bacteroids and are then capable of nitrogen fixation (31). Finally, the cortical layer of the plant root proliferates to form structures called nodules that contain the symbiotic bacteria.

The flagella of *S. meliloti*: similarities and differences to *E. coli* flagella

The flagella of *E. coli* and *S. meliloti* are different in both composition and mode of rotation. Based on differences observed under the electron microscope, bacterial flagella are classified as plain and complex. *E. coli* flagella have a smooth surface appearance with faint striations and are classified as plain (75). *S. meliloti* flagella however, have a helical pattern of alternating ridges and grooves and are classified as complex (36). Additionally, *S. meliloti* flagella consist of four flagellin subunits: FlaA, FlaB, FlaC and FlaD, with FlaA as the major flagellin present in the filament (72). Complex flagella are more rigid and locked in a right-handed helix (22). This allows the *S. meliloti* cells to swim in highly viscous media, which is advantageous to their survival in a soil environment. Also, different from the *E. coli* flagellar motor that switches between counter clockwise and clockwise rotation, flagellar rotation in *S. meliloti* is unidirectionally clockwise, and swimming cells respond to tactic stimuli by asynchronous deceleration and stops of individual filaments, resulting in a dissociation of the propulsive bundle (22, 71) (Figure 1.1). When individual flagellar motors reduce their rotational speeds, the flagellar bundle breaks up and the bacterium tumbles.

The mentioned unidirectional rotation and speed variation of the *S. meliloti* flagellar motor are new features that find their place in the presence of new motility genes. In addition to *motA* and *motB*, whose products function in analogy to their *E. coli* counterparts by

regulating ion flow across the inner membrane and coupling the flow of protons to flagellar rotation, *S. meliloti* possesses two additional motility genes *motC* and *motE* (16, 61). MotC is a periplasmic protein that is believed to facilitate the proton flow through the MotA/MotB channel. MotE serves as specific chaperone for the periplasmic MotC by ensuring correct folding and stability of MotC (16).

Diverse modes of signal termination

Though signal termination in two component regulation by the action of a phosphatase (CheZ in *E. coli*) is the best understood system so far, various bacteria have evolved different ways to affect signal termination. Other phosphatase families such as the CheC-type family and Rap family show different modes of response regulator dephosphorylation with a common catalytic theme (63, 67). First identified in *Bacillus subtilis*, the CheC-type family includes the phosphatases CheC, CheX and FliY (92). Though these proteins have very divergent amino acid sequences overall, they all have the conserved D/S-X3-E-X2-N-X22-P motif, in which the conserved glutamate residue is necessary for CheY association and the conserved asparagine residue is necessary for phosphatase activity. The glutamate and asparagine residues probably function like the catalytic aspartate and glutamine residues of CheZ (55). CheC-type family is more widespread than CheZ and is found in bacteria as diverse as firmicutes, thermotogales, proteobacteria and spirochetes (93). The RapH protein was shown to dephosphorylate the response regulator Spo0F in *Bacillus subtilis* (57).

The reverse flow of phosphate groups from a phosphorylated response regulator to its cognate kinase in a two-component system, first described by Sourjik and Schmitt, is called retrophosphorylation (84). Retrophosphorylation as a means to cause signal termination

has also been observed in *Helicobacter pylori* (30). In this organism, no CheZ homolog is present and thus, CheY1 transfers its phosphate group back to CheA with the CheY2 protein acting as a phosphate sink. Three CheV proteins also serve to dephosphorylate CheA~P and aid in maintaining control on activated CheY1 (30).

Regulation of chemotaxis in *S. meliloti*

Some members of the α-subgroup proteobacteria members contain more than one response regulator protein, in conjunction with the absence of the phosphatase CheZ. The signal transduction chain of *S. meliloti* involves two response regulators, CheY1 and CheY2, both are phosphorylated by CheA (Figure 1.4). CheY2-P is the main regulator of motor function and causes a decrease of rotary speed of the unidirectional CW-rotating flagellar motor resulting in tumbling motility (71). CheY2-P retro-transfers its phosphoryl group to CheA, which in turn phosphorylates CheY1 (84). CheY1 thus acts as a sink for phosphoryl groups from CheY2-P and emulates the role of the phosphatase CheZ. This mechanism now appears as a general feature in the chemotactic signaling chain of the α-subgroup of proteobacteria. The back-shuttling of the phosphoryl group to CheA is unique for CheY2-P; neither CheY1-P from *S. meliloti* nor CheY-P from *E. coli* exhibits this behavior.

The possible role of CheS in signal termination

The *che* operon in *S. meliloti* consists of ten genes coding for various constituents of the chemotaxis signaling chain. It contains two small open reading frames of unknown function, *orf2*, which is located between the genes coding for *icpA*, and the response regulator *cheY1*, and *orf10*, which is located 3' or the chemotaxis gene *cheD* (Figure 1.5) (23). *orf2* is now named *cheS*. CheS is a 10-kDa protein and has distinct similarities with the derived amino acid sequences of non-assigned genes from other α-proteobacteria. The

chemotaxis operon arrangement of these proteobacteria is also very similar to that of the *che1* operon of *S. meliloti*. Earlier work on *che*-gene mutants showed that *cheS* and *cheY1* mutants had same swimming speed phenotype. The Δ*cheS* strain exhibits a 25% reduction of chemotaxis and swimming motility on Bromfield swarm plates, similar to a strain lacking *cheY1*. Both Δ*cheS* and Δ*cheY1* mutant strains swam about 8 μm/s slower than the wild type strain (64). Also, crosslinking experiments of CheS with other proteins in the chemotaxis chain indicated that CheS interacts with CheA. Confocal microscopy showed that CheS-eGFP is localized at the cell pole together with the chemotaxis cluster (100). Hence,

1. The Δ*cheS* strain exhibits a slower swimming phenotype similar to the phenotype exhibited for Δ*cheY1* which indicates that CheS participates in the process of signal termination by removing phosphate groups from activated CheY2 in a CheA dependent manner
2. CheS interacts with CheA and the $P2_{linker}$ domain of CheA, as established by crosslinking experiments
3. CheS is co-expressed in a stable, soluble form in the presence of CheA or the $P2_{linker}$ domain, and
4. CheS is localized at the polar chemotaxis cluster of *S. meliloti* in a CheA-dependent manner.

Data from behavioral, *in vitro* and *in vivo* studies suggested a possible role of CheS in signal termination. The goal of my research was to determine the role of CheS in chemotactic signal termination in *S. meliloti* and the results of my work are presented in this thesis.

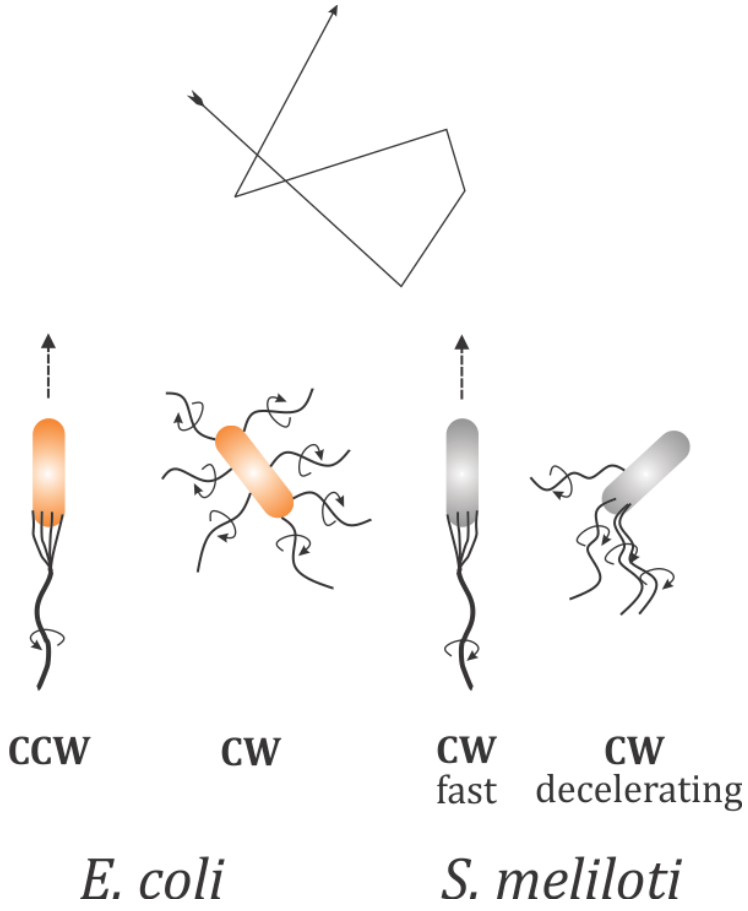

Figure 1.1. Modes of chemotactic motility in *E. coli* and *S. meliloti.* Top: The general swimming pattern of flagellated bacteria consists of alternating runs and tumbles. Bottom: Modes of flagellar rotation during runs and tumbles. Adapted from Scharf and Schmitt (71). Counter-clockwise rotation is abbreviated as CCW and clockwise as CW.

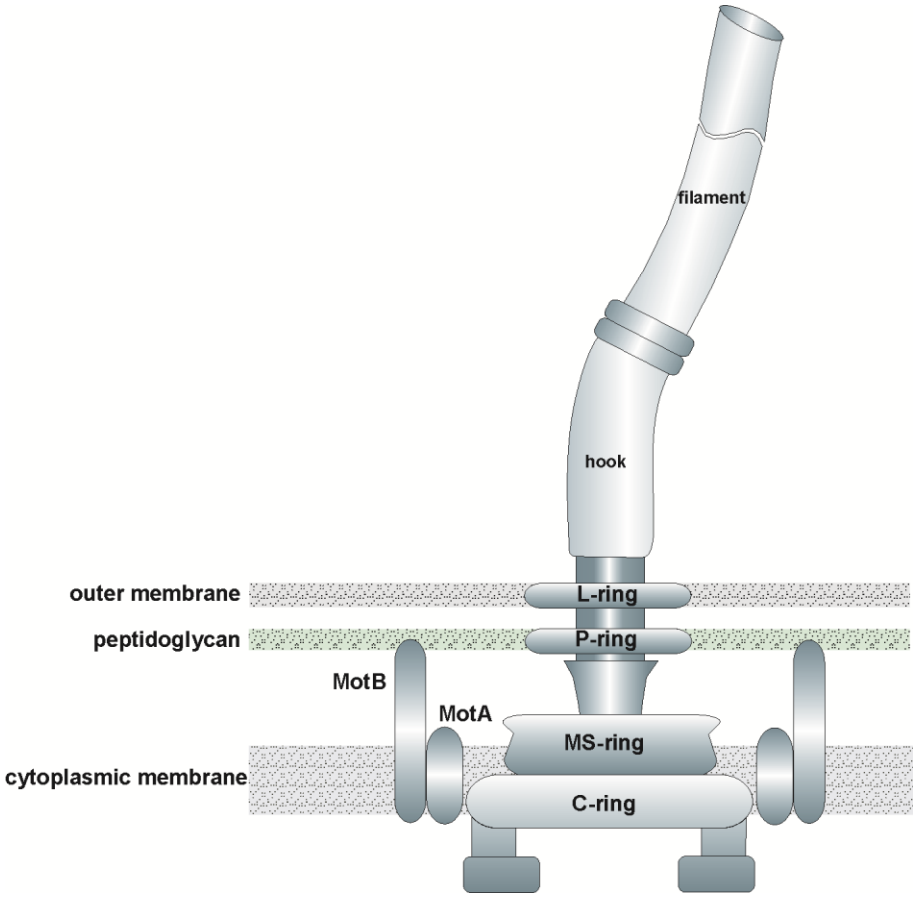

Figure 1.2. A schematic diagram of the *Escherichia coli* flagellar motor. L-ring for *l*ipopolysaccharide, P-ring for *p*eptidoglycan, S-*s*upramembrane and M-*m*embrane form the MS ring, and C-ring for *c*ytoplasm form the flagellar motor. The L and P rings do not rotate and form bearings to support the rod. The transmembrane stator proteins MotA and MotB form torque-generating units surrounding the rotating part of the motor. The hook assembly holds the flagellar filament in place and provides a flexible hinge to the filament. Figure courtesy Dr. Scharf.

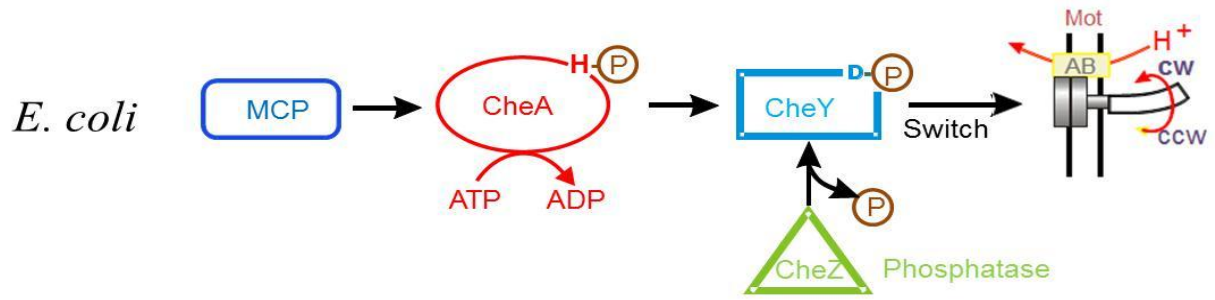

Figure 1.3. Schematic of the chemotactic signaling chain in *Escherichia coli*. It is composed of MCPs, a histidine autokinase CheA and a single response regulator CheY regulating flagellar rotation. CheA is auto-phosphorylated at the conserved His residue upon detecting a change of the methylation state of the receptor. This phosphate is transferred to the response regulator at a conserved Asp residue. Phosphorylated CheY~P binds to the C ring of the flagellar motor and switches rotation from CCW to CW. The phosphatase CheZ dephosphorylates CheY~P and maintains the balance of CheY vs. CheY~P in the system to modulate chemotactic motility. Image courtesy Dr. Scharf.

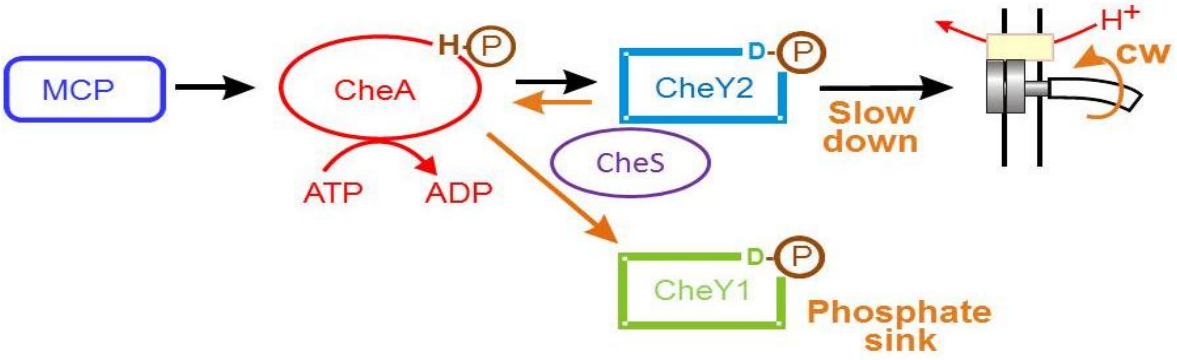

Figure 1.4. Schematic of the chemotactic signaling chain in *Sinorhizobium meliloti*. It is composed of MCPs, a histidine autokinase CheA and response regulators CheY2 (regulating flagellar rotation) and CheY1 (acting as a phosphate sink for signal termination). CheA is auto-phosphorylated at the conserved His residue upon detecting a change of the methylation state of the receptor. This phosphate is transferred to the response regulator CheY2 at a conserved Asp residue. Phosphorylated CheY2~P binds to the C ring of the flagellar motor and modulates rotation speed of the flagellar motor. CheY2~P can retro-transfer its phosphate to CheA, which can then transfer the phosphate to CheY1, which acts as a phosphate sink to modulate chemotactic motility. Image courtesy Dr. Scharf.

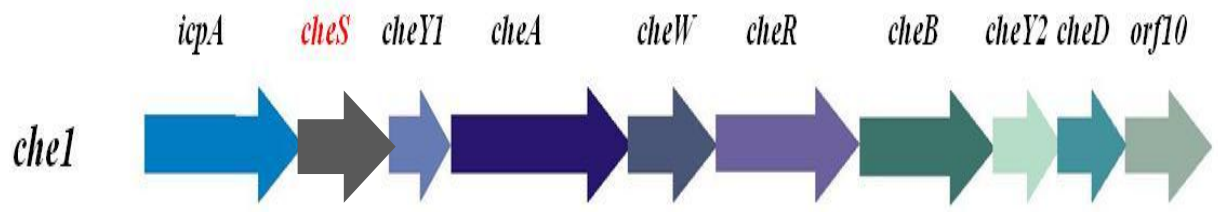

Figure 1.5. Organization of the *S. meliloti* chemotaxis operon *che1*. *cheS* is annotated as *orf2* and is the second gene located 3' of the gene coding for the soluble receptor *icpA. orf10* is the tenth gene in the operon and is found 3' of the gene coding for the chemoreceptor-glutamine deamidase, CheD. Image courtesy Dr. Scharf.

Chapter 2

Analysis of the properties of CheS and its interaction with CheA

Abstract

The gene coding for CheS was earlier annotated as *orf2*. CheS was predicted to be a 97 amino acid residue protein with a molecular weight of 10.3 kDa and a pI of 5.02. The amino acid sequence of CheS bears distinct similarities to the predicted amino acid sequences of proteins encoded by unassigned genes from other α-proteobacteria. Sequence conservation is higher at the α4 and α5 helices. Fluorescence microscopy confirmed the localization of CheS at the polar chemotaxis cluster in a CheA-dependent manner. Co-localization of CheS and CheA was also demonstrated by fluorescence microscopy. Double deletion mutants Δ*cheS*Δ*cheA* and Δ*cheS*Δ*cheY2* exhibited motility behavior equivalent to the control mutants Δ*cheA* and Δ*cheY2* on swim plates, let suggest that CheS may regulate intracellular CheY2~P concentration and does not act independently on the flagellar motor. Since the interaction of CheS with CheA and with the P2 domain was already established, efforts were made to confirm this interaction through immunoblots. Further insights into the binding region of CheS at the P2 domain were obtained from limited proteolysis with chymotrypsin and thermolysin, and subsequent analysis of the stable fragments by MS/MS. CheS was found to bind to $CheA_{163-256}$. This binding domain overlaps the N-terminal half of the CheY2 binding domain ($CheA_{174-316}$). CheS interaction with the CheY2 binding domain was proved by successful co-expression and co-purification of the His_6-$CheA_{174-316}$/CheS complex.

Materials and methods

Bacterial strains and plasmids

E. coli K-12 and *S. meliloti* RU11/001 derivatives were used in this study. These derivative strains and plasmids are listed in Table 2.1. Plasmids used for protein expression were derivatives of pET27bmod or pTYB1.

Media and growth conditions

E. coli strains were grown in Luria broth (LB) medium at 37°C. *S. meliloti* strains were grown in Tryptone-Yeast extract-Calcium chloride (TYC) broth (0.5% tryptone, 0.3% yeast extract, 0.13% $CaCl_2$ x $6H_2O$ [pH 7.0]) at 30°C (61) for two days. For fluorescent microscopy and motility analysis, stationary phase cultures of *S. meliloti* were diluted 1:50 in 10 ml RB minimal medium (6.1mM K_2HPO_4, 3.9mM KH_2PO_4, 1mM $MgSO_4$, 1mM $(NH4)_2SO_4$, 0.1mM $CaCl_2$, 0.1mM NaCl, 0.01mM Na_2MoO_4, 0.001mM $FeSO_4$, 20µg/l biotin, 100µg/l thiamine) (22), layered on Bromfield agar plates (83), and incubated at 30°C for 20 hours. Specific to the plasmid resistance gene in *E. coli*, the following antibiotics were used at the indicated final concentrations: ampicillin at 100µg/ml and kanamycin at 50µg/ml. For *S. meliloti* strains, streptomycin was used at 600µg/ml.

Alignment of polypeptide sequences

The predicted amino acid sequence of CheS (protein ID: AAA86672.1) was extracted from PUBMED (http://www.ncbi.nlm.nih.gov/pubmed/). A position-specific iterated BLAST search (PSI-BLAST) was performed to identify homologs of CheS in other bacteria and returned several hits with 70-100% query coverage. These sequences, most of which belonged to members of the α-proteobacteria were extracted from PUBMED and aligned

using the multiple sequence alignment function on the LaserGene MegAlign™ program (DNAStar) running the CLUSTAL-W algorithm (96). The arrangement of the chemotaxis operons of these α-proteobacteria was confirmed to be similar to that of the chemotaxis operon *che1* of *S. meliloti* RU11/001 in which, the CheS orthologs were encoded by the second gene on the operon. The aligned residues were color coded to display identity. The color coding scheme was based on the nature of the residues, in which, hydrophobic residues (Ile, Val, Leu, Phe, Tyr and Trp) and residues with small functional groups (Pro, Ala, Gly and Ser) were grouped together. Pairwise alignment of each derived protein sequence with *S. meliloti* CheS was also obtained using MegAlign to determine percent identity between each pair.

Secondary structural elements of the CheS protein were predicted using the PSIPRED server (47), and results obtained from that analysis were added to the multiple sequence alignment.

Motility assays

Swim plates containing Bromfield medium and 0.3% Bacto Agar were inoculated with 3µl of stationary phase test cultures and incubated at 30°C for four days. Chemotactic efficiency was determined by measuring the swim diameter at the point of inoculation on the plate. All plates were inoculated in duplicate for each liquid culture used. Swimming speed of the mutants was estimated by observing motile cultures under 40X magnification. The results were analyzed on Microsoft Excel 2010.

Expression and purification of proteins

Recombinant His_6-CheS, His_6-CheA, His_6-CheA/CheS, His_6-P1/CheS, His_6-$P2_{linker}$, His_6-$P2_{linker}$/CheS, His_6-P345/CheS and His_6-$CheA_{174-316}$/CheS were over-expressed in *E. coli* BL21DE3 cells from respective plasmids (Table 2.2). Cells were grown at 37°C in Luria broth containing 40µg/ml kanamycin to an OD_{600} between 0.7 to 0.8 and gene expression was induced by the addition of 0.3mM isopropyl-β-D-thiogalactopyranoside (IPTG). Cultivation was continued for 16h at 16°C in an Innova™ 4330 refrigerated shaking incubator (New Brunswick Scientific) till harvest. Cells were centrifuged at 8000 RPM for 8 minutes in the Avanti J-26 XP centrifuge (Beckman Coulter) at 4°C and the cell supernatant was discarded. The cell pellet was resuspended in cold binding buffer (20mM NaP_i, pH 7.4, 500mM NaCl and 20mM Imidazole) containing 10µl of 1mg/ml DNase I, 100µl of 100mM phenyl-methyl sulfonyl fluoride (PMSF) and 100µl of 100X Halt™-Protease Inhibitor cocktail (Thermo Scientific). Cells were lysed by at least three passages through a French pressure cell at 20,000 psi and the lysate was centrifuged at 21,500 RPM for 40 minutes at 4°C. Supernatant containing the soluble protein fraction was filtered through a low protein binding 0.2µm cellulose acetate membrane filter under vacuum and loaded on an ÄKTA chromatography system (GE healthcare) containing a 5ml Ni-NTA Hi-trap chelating column (GE Healthcare) that had been equilibrated with binding buffer at a flow rate of 5ml/minute. Proteins were eluted in a linear gradient of 15 bed volumes of elution buffer (20mM NaP_i, pH7.4, 500mM NaCl, 500mM imidazole, containing 50µl of 100X Halt-Protease Inhibitor cocktail (Thermo)) from 20mM - 500mM imidazole. Protein containing fractions were separated on a 15% (w/v) acrylamide gel containing SDS and pooled. The resulting pool was concentrated in an Amicon concentration cell under gaseous nitrogen

using the appropriate filter (10kDa cutoff for proteins containing CheA or P2 and 3kDa for proteins containing CheS). The concentrated proteins were filtered through a 0.2µm acetate syringe filter to remove aggregates and applied to a Hi-prep sephacryl S300 size exclusion column (GE Healthcare) equilibrated and developed with gel filtration buffer (20mM Tris/HCl pH7.5, 50mM NaCl, 1mM EDTA). Fractions containing proteins were electrophoretically separated on a 15% (w/v) acrylamide gel containing SDS to identify fractions containing the target protein. Fractions were pooled and proteins were concentrated on an Amicon cell as described above. Concentrated protein was filtered through a 0.2µm cellulose acetate syringe filter and concentration of the protein was determined by Bradford assay against a standard curve of known concentrations of bovine serum albumin (BSA). 10% (v/v) glycerol was added to the protein solutions, which were then aliquoted and flash-frozen on liquid nitrogen. The frozen proteins were stored at -80°C till further use.

Immunoblots

Expression and co-purification of CheS with various CheA domains was determined by immunoblotting and probing with α-CheS antibodies. Crude extracts of *E. coli* BL21DE3 cells containing expressed proteins were prepared as described above. To obtain similar amounts of expressed proteins, all cultures were normalized to an OD_{600} of 0.8 before lysis. 100µl of each lysate, representing the whole-cell fraction was removed and stored at 4°C. The remaining lysates were separated at 21,500 RPM for 40 minutes at 4°C in a refrigerated centrifuge, and the supernatant containing the soluble protein fraction was removed. 50µl of the soluble and whole-cell fraction was mixed with 10µl of 6X SDS-PAGE gel loading buffer and boiled at 95°C for 10 minutes. The samples were cooled on ice and

electrophoretically separated on Criterion 10-20% Tris/HCl gels (Bio-Rad), transferred to a 0.2µm PVDF membrane (Bio-Rad), and probed with affinity purified α-CheS polyclonal antibodies in a 1:100 dilution. The blot was then incubated with a mouse α-rabbit horseradish peroxidase-linked whole IgG antibody (GE Healthcare) at a dilution of 1:1000. Chemiluminiscence detection was achieved by developing the blot with SuperSignal® West Pico Chemiluminiscent ECL substrate (Pierce), and exposure to Hyperfilm ECL™ (GE Healthcare). The exposed films were developed with a SRX-101A medical film developer (Konica Minolta). Ni-NTA affinity purified CheA-domain/CheS complexes were also subjected to immunoblotting as described above.

Limited proteolysis and mass spectrometry

Limited proteolysis with chymotrypsin (Sigma) was performed at a protein concentration of 1 mg/ml in 1 mM EDTA, 50 mM NaCl, 20 mM Tris/HCl, pH 7.5 with a final concentration of 0.01 mg/ml chymotrypsin for 60 min at 37°C. Aliquots (20 µl) were withdrawn at 5, 20, 40, and 60 min and reactions were stopped by the addition of 10 µl of SDS-gel loading buffer. Limited proteolysis with thermolysin (*Bacillus thermoproteolyticus* Rokko, Sigma) was performed at a protein concentration of 0.5mg/ml in 4mM $CaCl_2$, 10% glycerol and 0.4 M NaCl, 20 mM Tris (pH 8.0), with a final concentration of thermolysin of 20µg/ml, 5µg/ml, 1.2µg/ml, 0.4 229µg/ml and 0.08µg/ml for 60 min at 37°C in a 20 µl reaction volume. Reactions were stopped by the addition of 0.5µl of 0.5M EDTA pH 8.0 and 10 µl of SDS-gel loading buffer. 30µl of each protein sample were separated on a Criterion 4-20% gradient acrylamide gel (Bio-Rad) and stained with Coomassie brilliant blue R250. Bands of interest were excised from the polyacrylamide gel and chopped into approximately 1 mm^3 pieces using a clean razor blade. MALDI-TOF MS/MS was performed on peptides contained in the

pieces which were prior digested with Asp-N, Trypsin or Chymotrypsin. Each MS/MS spectrum was typically the sum of approximately 1,500 individual laser shots. A peak list for each digest containing information from both the MS and MS/MS spectra was generated using the 4000 Explorer (AB Sciex) software.

Fluorescence microscopy

WT *S. meliloti* cells containing CheS-eGFP and CheS-eGFP/CheA-mRFP; and Δ*cheA S. meliloti* cells containing CheS-eGFP were grown in TYC broth containing 600µg/ml streptomycin, and motile cells were grown in minimal RB medium overlaid on Bromfield plates as described above. Cells were immobilized on clean slides coated with a 1% poly-L-lysine solution. 5µl motile cells from the mid-log phase were added to the slide and a coverslip was carefully placed on the droplet avoiding air bubbles. The coverslip was then sealed with an acrylic polymer to prevent drying of the slide. Images were obtained on an Olympus IX71 inverted fluorescence microscope, using a 100X NA 1.4UPlanSApo objective lens through a charge coupled device (CCD) camera (Photometrics CoolSNAP HQ2CCD) and analyzed using SoftWorx™ software (Applied Precision). The fluorescence signals from eGFP ($\lambda_{excitation}$ of 470nm) and mRFP ($\lambda_{excitation}$ of 580nm) were detected using FITC (525nm) and mCherry (630nm) filters respectively. WT *S. meliloti* cells were used as a control to detect background fluorescence in the eGFP excitation range.

Results and discussion

In silico analysis of CheS

The gene encoding CheS was earlier annotated as *orf2*, and in other members of the α-proteobacteria, its orthologs are annotated as *cheX*. This is one of the two open reading frames (ORF) of unknown function identified in the *che1* operon of *S. meliloti*, with *orf10* being the other gene of unknown function (23). *cheS* is located between the first gene of the operon, *icpA*, which encodes an internal chemotaxis protein and the gene encoding the response regulator CheY1. The predicted polypeptide sequence of CheS contains 97 amino acid residues with a molecular weight of 10.3 kDa and a pI of 5.02. It contains 20% hydrophilic and 34% hydrophobic residues. When the protein sequence of CheS was subjected to PSI-BLAST, a homology to the Sulfate Transporter/Anti-sigma factor Antagonist (STAS) domains (E value: 7.07e-04), found in sulfate transporters and anti-anti-sigma factors, such as SpoIIAA was observed (2). It has been reported that SpoIIAA is activated through phosphorylation of a conserved serine residue by the kinase SpoIIAB (44, 50). When the polypeptide sequences of CheS and its orthologs from other α-proteobacteria were aligned (Figure 2.1), a conserved Ser residue was identified at position 75. It is possible that CheS is phosphorylated by a yet known kinase in *S. meliloti* and this has to be further tested.

The multiple sequence alignment of *S. meliloti* CheS with its orthologs in other α-proteobacteria also revealed distinct similarities. A higher order of conservation of functional residues is seen in the α4 and α5 helices. Most of the residues found at these regions are hydrophobic in nature. The CheS protein from *S. meliloti* shows identities of

87% with *S. medicae*, 58% with *A. tumefaciens*, 56% with *R. leguminosarum*, 40% with *C. crescentus*, and 31% with *R. sphaeroides* encoded orthologs, respectively.

CheS regulates intracellular CheY2~P concentration

Since earlier experiments demonstrated that the phenotype of the *cheS* deletion strain was similar to that of the *cheY1* deletion strain, it was hypothesized that CheS may directly or indirectly regulate the intracellular concentration of CheY2~P and assist in signal termination. The swimming speed of the *cheY1* and *cheS* deletion strains was slower than the wild-type strain, which was due to higher CheY2~P concentration resulting in a higher rate of tumbles. Also, the swimming speed of *S. meliloti* cells carrying a *cheA* or *cheY2* deletion was observed to be higher than the wild type. This is due to the absence of CheY2~P, which results in a lower rate of tumbles. If CheS participates in decreasing the cellular CheY2~P concentration, then a double mutant of *cheS* with *cheA* or *cheY2* would result in a higher swimming speed, similar to the *cheA* or *cheY2* single mutant, and would prove that CheS does not act independently on the flagellar motor. The swim diameter on Bromfield plates (containing 0.3% agar) of the Δ*cheS*, Δ*cheA*, Δ*cheY2*, Δ*cheS*Δ*cheA* and Δ*cheS*Δ*cheA* mutant strains were compared to that of wild-type *S. meliloti* (Figure 2.2 and table 2.2). While the swim diameter of the c*heS* mutant showed a 10% reduction compared to the wild type strain, the swim diameters of *cheA, cheY2, cheScheA* and *cheScheY2* mutants were significantly reduced. However, when motile mutant cells were observed under the light microscope, their swimming speeds (Table 2.3) were higher than the wild type. Hence, the phenotypes of the mutant strains indicate that CheS does not act independently of CheY2~P and only regulates the cellular concentration of the activated response regulator.

CheS co-localizes with CheA at the chemotaxis cluster

It was established through confocal microscopy that the CheS-eGFP and CheA-mRFP fusion proteins localized at the chemotaxis cluster in *S. meliloti*, while CheS failed to localize in a *cheA* deletion mutant (100). My aim was to confirm these results and demonstrate the co-localization of CheS with CheA. Initially, the localization of CheS-eGFP and CheA-mRFP *in vivo* was established by fluorescence microscopy. The green signal from CheS-eGFP was detected at the cell poles in the area containing the polar chemotaxis cluster (Figure 2.3, A, C) (48). The red signal from mRFP was also found at the cell poles, essentially similar to earlier observations (Figure 2.3, D) (100). Also, CheS-eGFP emits a green signal and CheA-mRFP emits a red signal, and co-localized CheS and CheA would result in a yellow signal. It was observed that CheS and CheA both localized at the same pole (Figure 2.3, E). The localization of CheS at the cell pole in a CheA-dependent manner had also been demonstrated (100). I revisited the experiment, in which *S. meliloti* Δ*cheA* cells containing the expressed cheS-eGFP fusion were detected by fluorescence microscopy and observed using the FITC filter by excitation. CheS-eGFP was found to be uniformly distributed in the cell and was no longer localized at the cell pole in the absence of CheA, confirming earlier observations (Figure 2.3, B) (100). For all the experiments *S. meliloti* RU11/001 was used as a control to determine background signal arising from FAD and FMN in the green region of the spectrum, which could interfere with the eGFP signal (data not shown). These experiments confirm the fact that CheS localizes at the chemotaxis cluster in a CheA-dependent manner and indicate the co-localization of CheS and CheA in the cell.

CheS is stably expressed in the presence of CheA

To confirm the expression and co-purification of CheS with CheA, as had been proven by Purschke in 2007 (64), His_6-CheS and His_6-CheA were expressed as controls, in addition to the His_6-CheA/CheS complex to perform immunoblot analysis. Post expression of the proteins, cells were lysed using a French pressure cell, 100µl of the lysate was removed and preserved at 4°C till further use and the remainder was separated by centrifugation. The soluble protein fraction obtained in the supernatant was labeled S and the whole cell lysate labeled C in Figure 2.4. After resolution on a Criterion 4-20% gradient acrylamide gel followed by immunoblotting, the bands were probed by α-CheS antibodies (Figure 2.4, A and B). The His_6-CheA/CheS protein complex that had been co-expressed and co-purified by Ni-NTA affinity chromatography was also probed with α-CheS antibodies as described above (Figure 2.4, B). The purified CheA/CheS complex was also separated electrophoretically and stained with Coomassie brilliant blue (Figure 2.4, C). CheS was stably expressed in the presence of CheA only (Figure 2.4, A, lane 2, B, and C). CheA was used as an internal control to rule out cross-reactivity of the α-CheS antibody with CheA (Figure 2.4, A, lane 5).

CheS is stably expressed with the P2 domain of CheA

Interaction of the P2 domain of CheA with CheS had been established by cross-linking experiments (64), following which, the His_6-$P2_{linker}$/CheS complex was co-expressed and co-purified (B. Scharf, personal communication). The stable expression of CheS with different domains of CheA, including P2 was confirmed by immunoblot. CheA is an 81-kDa protein and contains five domains: P1, responsible for phosphotransfer and containing the conserved His residue, P2, response regulator binding domain which interacts with CheY2

and CheB, P3, dimerization domain which helps the CheA monomers associate to form a dimer, P4, catalytic domain responsible for ATP binding and hydrolysis and P5, sensor domain responsible for binding to the MCP via the adapter protein CheW (Figure 2.5). These domains were defined using the domain structure of *E. coli* CheA as a template (11, 29, 88, 91, 101). The fact that individual domains of CheA could be stably expressed was already established (21, 25, 64, 66). The same approach that had been used earlier to confirm the stable expression and purification of CheS with CheA was used to study the expression and purification of CheS with CheA domains. From existing plasmid constructs, CheS was co-expressed with His_6-P1 (aa 1-135; 16.1 kDa), His_6-$P2_{linker}$ (aa 120-360; 26.9 kDa) and His_6-P345 (aa 355-758; 44.5 kDa) domains. Post expression of the domain/CheS complex, cells were lysed using a French pressure cell, 100µl of the lysate was removed and preserved at 4°C till further use and the remainder was separated into a soluble fraction and an insoluble fraction by centrifugation. After resolution on an SDS-PAGE gel followed by immunoblotting, the blot was probed with α-CheS antibodies (Figure 2.6, A). His_6-P1, $P2_{linker}$ and P345 domains in complex with CheS were also co-purified by Ni-NTA affinity chromatography and probed with α-CheS antibodies (Figure 2.6 B). Purified fractions were also separated electrophoretically and stained with Coomassie brilliant blue (Figure 2.6, C). CheS was stably expressed in the presence of the $P2_{linker}$ domain only (Figure 2.6, A, lanes 3+4, B, lane 2, and C, lane 2). The ~60-kDa band was observed on the immunoblot which indicated a combined molecular weight of the $P2_{linker}$ and CheS. CheS did not stably express with the P1 domain (Figure 2.6, A, lanes 1+2; B, lane 1, and C, lane 1) or with the P345 domain (Figure 2.6, A, lanes 5+6, B, lane 3, and C, lane 3). It should be noted that $P2_{linker}$ produced a band at ~37-kDa on the SDS-PAGE gel that is 10-kDa larger than predicted

from the amino acid sequence. The apparent molecular weights of His_6-CheA, His_6-P1 and His_6-P345 were similar to their predicted molecular weights. We determined the molecular weight of His_6-$P2_{linker}$ by MALDI MS and obtained a value of ~27kDa which was close to the calculated mass of 26,601 Da. The reason for the anomalous behavior of His_6-$P2_{linker}$ could only be speculated, but the predicted pI of this protein is 4.4 and could account for the low electrophoretic mobility (45). A weak CheS band was observed in Figure 2.6 (B, lane 3) which could represent a low-abundance complex of P345 with CheS, and could imply that the P345 domain weakly interacts with CheS. This band disappeared when the protein samples were boiled prior to loading on the SDS-PAGE gel (data not shown). Therefore, it was established that the $P2_{linker}$ domain is the major interacting surface for CheS and P345 contains a weak interaction surface not capable of promoting stable expression of CheS.

The CheS binding domain is $CheA_{163\text{-}256}$

After confirming the interaction of CheS with the $P2_{linker}$ domain of CheA, an effort was made to determine the accurate interaction surface of CheS with the P2 domain. Limited proteolysis is an analytical technique that can be used to study protein-protein interaction by observing the protective effect of a protein on another protein from proteolytic enzymes such as trypsin, chymotrypsin or thermolysin. The PeptideCutter program on EXPASY was used to predict proteolytic cleavage sites in $P2_{linker}$ for chymotrypsin, which cleaves C-terminal of Phe, Trp and Tyr residues, and for thermolysin, which cleaves N-terminal of Leu and Phe (102). The results of the predicted proteolytic cleavage sites of chymotrypsin (high-specificity) and thermolysin on the His_6-$P2_{linker}$ polypeptide sequence are presented in Figure 2.7. For thermolysin 70 cleavage sites were predicted while chymotrypsin recognizes 14 sites in $P2_{linker}$. Low protease concentration and limited incubation time are

used to limit proteolysis of the target protein, resulting in the formation of a stable digestion product that has been protected from proteolysis by an interacting protein. The time course of proteolysis, as monitored by SDS-PAGE is shown in Figure 2.8, A. and B. CheS was unaffected by proteolysis, and thus it can be inferred that CheS has a compact structure. Two stable fragments of the His_6-$P2_{linker}$/CheS complex were obtained with chymotrypsin (C2, C3) and thermolysin (T2, T3), respectively (Figure 2.8, A and B). From the results obtained by Matrix assisted LASER desorption-ionization, time of flight (MALDI-TOF) mass spectrometric analysis of the cleaved fragments, C2 was aa 120-151, C3 was aa 163-256, T2 was aa 158-283 and T3 was aa 158-260. The stable CheS-binding domain was defined to contain residues 163-256 ($CheA_{163-256}$) (Figure 2.8, C). The CheS-binding domain was obtained by overlapping the chymotrypsin fragment C3, with five N-terminal and four C-terminal residues from the thermolysin fragment T3. As a control, the His_6-$P2_{linker}$ domain was subjected to limited proteolysis under the same conditions, and no stable fragment was observed (Figures 2.8, A. and B., even numbered lanes). Therefore, CheS was found to bind to the central P2 domain, $CheA_{153-256}$, rendering it insensitive to proteolytic degradation. It had been established earlier that CheY2 binds to the P2 domain at a site overlapping the C-terminal half of the CheS binding domain (66). This could indicate a possible role of CheS in the phosphotransfer events between CheA and CheY2.

CheS can be stably expressed with $CheA_{174-316}$

An effort was made to co-express and co-purify the $CheA_{174-316}$/CheS protein complex, which was co-expressed as described above and purified by Ni-NTA affinity chromatography. Notably, $CheA_{174-316}$ is the CheY2 binding domain and since this domain overlaps the CheS binding domain at $CheA_{163-256}$, it was hypothesized that CheS would express stably with the CheY2 binding domain (66). The $CheA_{174-316}$/CheS complex was obtained and separated on an SDS-PAGE gel (Figure 2.9). The stable expression of CheS with the $CheA_{174-316}$ domain confirms the inclusion of the CheS-binding domain.

Conclusions

Multiple sequence alignment of the polypeptide sequence of CheS from *S. meliloti* with derived polypeptide sequences of its orthologs from other α-proteobacteria displayed shared characteristics, including a conserved central domain rich in hydrophobic residues and a conserved Ser residue at position 75. A STAS domain was also identified in the CheS protein. Analysis of *cheS, cheA, cheY2, cheScheA* and *cheScheY2* deletion strains in comparison with the *S. meliloti* wild-type strain indicated that the observed chemotaxis and swimming speed phenotypes were not caused by the *cheS* deletion. Also the *cheA* and cheY2 mutants were dominant over the *cheS* phenotype. This indicates that CheS does not regulate chemotaxis and motility, and only regulates the intracellular concentration of CheY2~P similar to the effect of CheY1. The localization of CheS at the polar chemotaxis cluster in a CheA-dependent manner was confirmed by fluorescence microscopy. Also, the co-localization of CheS and CheA was demonstrated. The stable expression of CheS with CheA or the CheA-P2 domain was confirmed by immunblots. CheS did not stably express in isolation or with the P1 and P345 domains of CheA. Further analysis of CheS binding to CheA determined the CheS interaction surface to be $CheA_{163-256}$, which overlaps with the CheY2 binding domain ($CheA_{174-316}$) on the P2 domain. To prove that CheS interacts with its binding domain, CheS was stably expressed with the $CheA_{174-316}$ domain, which includes $CheA_{163-256}$. This stable interaction indicates that CheS may function through its association with the P2 domain of CheA.

Table 2.1. Bacterial strains

Strain	Relevant characteristics [a]	Source or reference
Strain		
E. coli DH5α	*recA1 endA1*	(26)
ER2566	*Ion ompT lacZ::T7*	New England Biolabs
BL21(DE3)	F^- *ompT hsdS*$_B$ (r_{B^-} m_{B^-}) *gal dcm* λ(DE3)	Novagen
M15/pREP4	Km^r; *lac ara gal mtl F recA uvr*	Qiagen
S17-1	*recA endA thi hsdR* RP4-2 Tc::Mu::Tn7 Tp^r Sm^r	(82)
S. meliloti		
BS147	Sm^r; Δ*cheS*Δ*cheA*	B. Scharf
BS151	Sm^r; *cheS*-eGFP, Δ*cheA*	J. Hughes
BS154	Sm^r; *cheS*-eGFP, *cheA*-mRFP	J. Hughes
RU11/001	Sm^r; spontaneous streptomycin-resistant wild-type strain	(62)
RU11/310	Sm^r; Δ*cheA*	(83)
RU11/307	Sm^r; Δ*cheY2*	(83)
RU11/408	Sm^r; Δ*cheS*	P. Muschler
RU13/260	Sm^r; Δ*cheS*Δ*cheY2*	E. Schilling
RU13/280	Sm^r; *cheS*-eGFP	(64)
RU13/311	Sm^r; *cheA*-mRFP	(66)

[a] Nomenclature according to Bachmann (8) and Novick et al. (52)

Table 2.2. Bacterial plasmids

Plasmid	Expressed protein	Relevant characteristics [a]	Source or reference
Plasmid			
pET27bmod	None	Km^r, derivative of pET27	R. Seidel, MPI Dortmund
pQE30	None	Ap^r, expression vector	Qiagen
pTYB1	None	Ap^r, expression vector	New England Biolabs
pBS16	CheY1	Ap^r, 360 bp *Nde*I-*Sap*I PCR-fragment containing *cheY1* cloned into pTYB1	B. Scharf
pBS18	CheY2	Ap^r, 387 bp *Nde*I-*Sap*I PCR-fragment containing *cheY2* cloned into pTYB1	B. Scharf
pBS173	CheS w/o His tag	Km^r, 291 bp *Nco*I/*Bam*HI fragment from pRU2804 cloned into pET27bmod	B. Scharf
pBS174	His_6-CheA/CheS	Km^r, 2321 bp *Eco*RI/*Hin*dIII fragment from pRU1742 containing the promoter region of pQE30 and His_6-*cheA* cloned into pBS173	B. Scharf
pBS175	His_6-$P2_{linker}$	Ap^r, 720 bp *Bam*HI/*Hin*dIII PCR-fragment containing *cheA*- $P2_{linker}$ (120-360 aa) cloned into pQE30	B. Scharf
pBS295	His_6-CheA	Km^r, 2321 bp *Eco*RI/*Hin*dIII fragment from pRU1742 containing the promoter region of pQE30 and His_6-*cheA* cloned into pET27bmod	B. Scharf
pBS330	His_6-P2/CheS	Km^r, 764 bp kb *Eco*RI/*Hin*dIII fragment containing the promoter region of pQE30 and His_6-*cheA*-$P2_{linker}$ in pET27bmod	B. Scharf
pBS335	His_6-P1	Ap^r, 408 bp *Bam*HI /*Hin*dIII PCR-fragment containing *cheA*-*P1* (1-135 aa) cloned into pQE30	B. Scharf
pBS339	His_6-P345/CheS	Km^r, 1256 bp *Eco*RI/*Hin*dIII fragment from pBS1001 containing the promoter region of pQE30 and His_6-*cheA*-*P345* in pBS173	B. Scharf
pBS1001	His_6-P345	Ap^r, 1256 bp *Bam*HI-*Hin*dIII fragment containing the P3P4P5 domains of CheA in pQE30	J. Hughes
pRU1742	His_6-CheA	Ap^r, 2321 bp *Bam*HI-*Hin*dIII fragment containing His_6-CheA cloned into pQE30	(84)
pRU2804	CheS	Ap^r, 291 bp *Eco*RI-*Bam*HI PCR-fragment containing *orf2* cloned into pQE60	B. Scharf

[a] Nomenclature according to Bachmann (8) and Novick et al. (52)

Table 2.3: Chemotactic behavior of *S. meliloti* wild type and mutant strains

Strain	swim size[a] (% wild-type)	standard deviation (%)	Motility[b]
RU11/001 (wt)	100	±30	++
RU11/408 (Δ*cheS*)	91	±25	++
RU11/307 (Δ*cheY2*)	31	±17	+++
RU11/310 (Δ*cheA*)	37	±11	+++
RU13/260 (Δ*cheS*Δ*cheY2*)	36	±8	+++
BS147 (Δ*cheS*Δ*cheA*)	34	±9	+++

[a] Swim diameters are listed relative to the swim diameter of the wild-type strain on a 0.3% Bromfield agar plate after 4 days at 30°C. Values represent averages from 10 replicates.

[b] Motility values are indicated as a function of swimming speed of the test organisms as observed under 40X magnification.

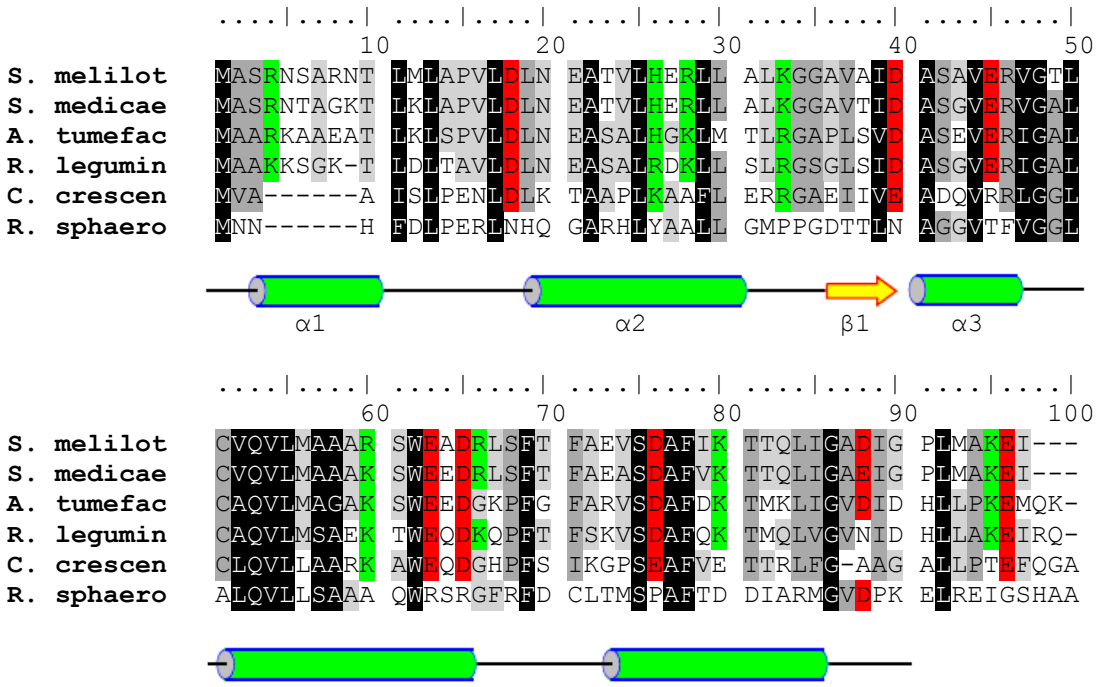

Figure 2.1. Alignment of six polypeptide sequences of CheS and its orthologs. Sequences from *Sinorhizobium meliloti* (U13166.1), *Sinorhizobium medicae* (YP_001325927.1), *Agrobacterium tumefaciens* (NP_353544.1), *Rhizobium leguminosarum* (YP_766296.1), *Caulobacter crescentus* (NP_419250.1), and *Rhodobacter sphaeroides* (YP_001167990.1) (GenBank accession numbers in parentheses). Sequences were subjected to multiple sequence alignment using the CLUSTAL-W algorithm on MegAlign. Sequence identities of 100%, 83% and 47% are shaded black, dark grey and light grey. Identical acidic and basic amino acids are shaded red and green respectively. A scale represents the number of amino acids in each line and dashes indicate gaps. Predicted secondary structure elements according to PSIPRED are appended below the sequences (47). Green cylinders indicate α-helices, yellow arrows β-sheets and black lines coils.

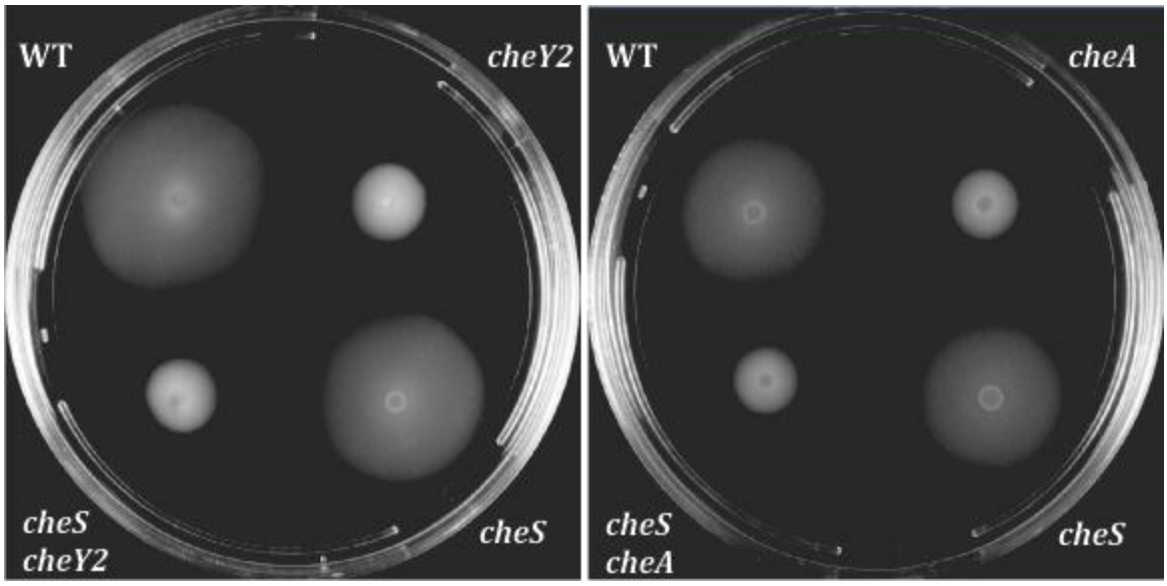

Figure 2.2. Swim plates showing phenotypes of *S. meliloti* WT and several deletion mutants. 3µl of cultures grown to stationary phase in TYC medium containing streptomycin were spotted on Bromfield swarm plates and incubated at 30°C for 4 days. The resulting swim circles are presented.

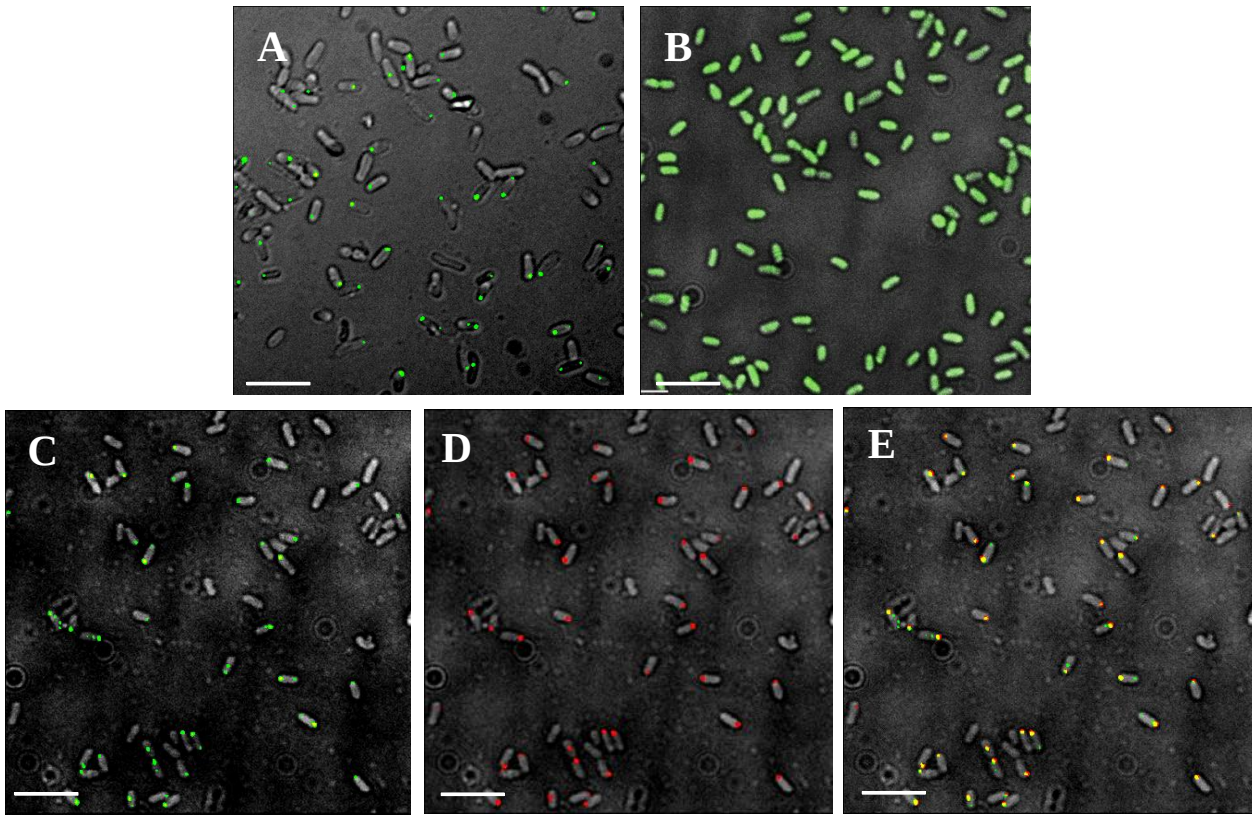

Figure 2.3. Localization of CheS and CheA in *S. meliloti* cells by fluorescence microscopy. CheS fused to eGFP (enhanced green fluorescent protein) and CheA fused to mRFP (monomeric red fluorescent protein) were monitored in wild-type and mutant backgrounds. **A.** CheS-eGFP in WT cells; **B**. CheS-eGFP in Δ*cheA* cells; **C**. CheS-eGFP in WT cells; **D**. CheA-mRFP in WT cells; **E.** CheS-eGFP and CheA-mRFP in WT cells (overlay of C and D). White bars correspond to 5μm.

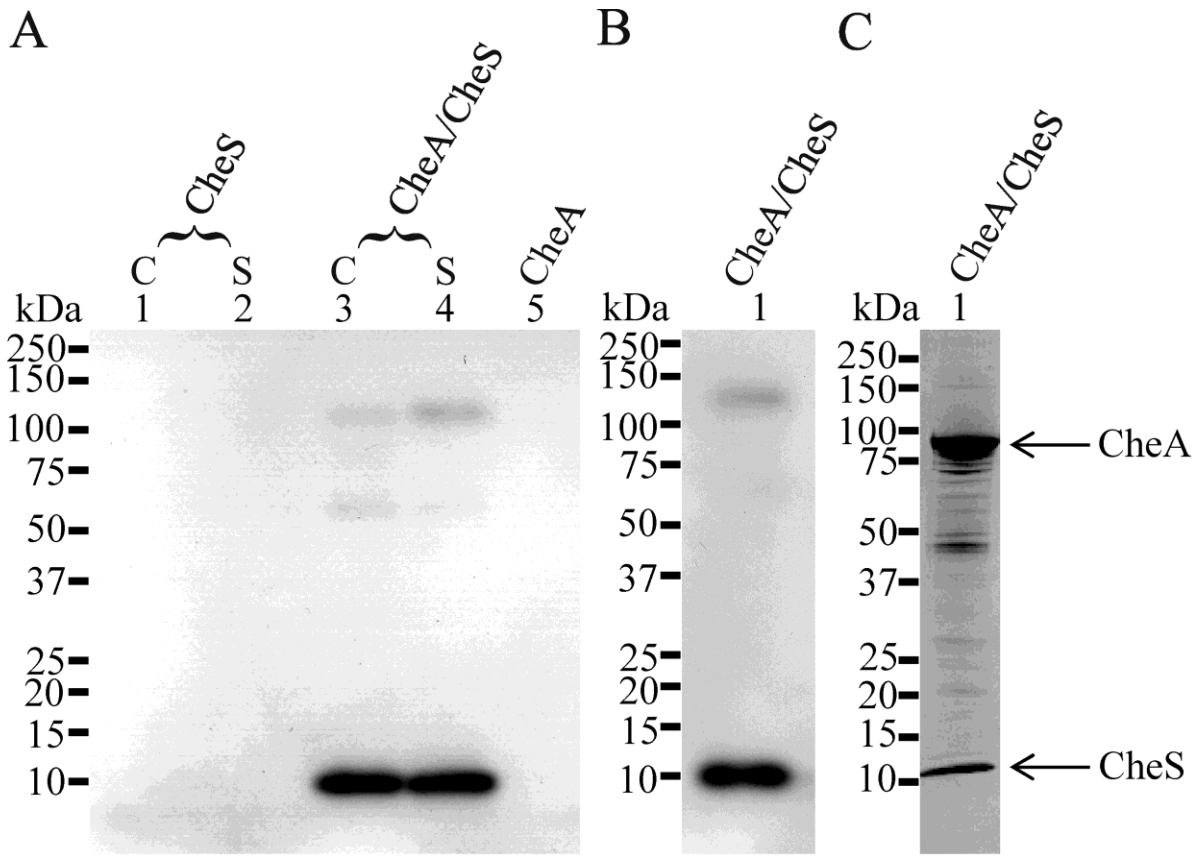

Figure 2.4. SDS-PAGE and immunoblots to assess co-expression and purification of CheS and His_6-CheA. **A.** Equal volumes of cell extracts and soluble fractions were separated on a 10-20% SDS-gel, transferred onto PVDF membrane and probed with anti-CheS antibody. Lanes 1+2: Whole cell extract (C) and soluble fraction (S) of *E. coli* BL21DE3 (pBS173) expressing CheS; Lanes 3+4; Whole cell extract and soluble fraction of *E. coli* BL21DE3 (pBS174) expressing CheS and His_6-CheA; Lane 5: His_6-CheA as control. **B** and **C.** Proteins after chromatography on Ni-NTA Sepharose were separated on a 10-20% SDS-gel, and **B.** transferred onto PDVF membrane and probed with anti-CheS antibody; or **C.** stained with Coomassie brilliant blue. Lane 1: CheA/CheS.

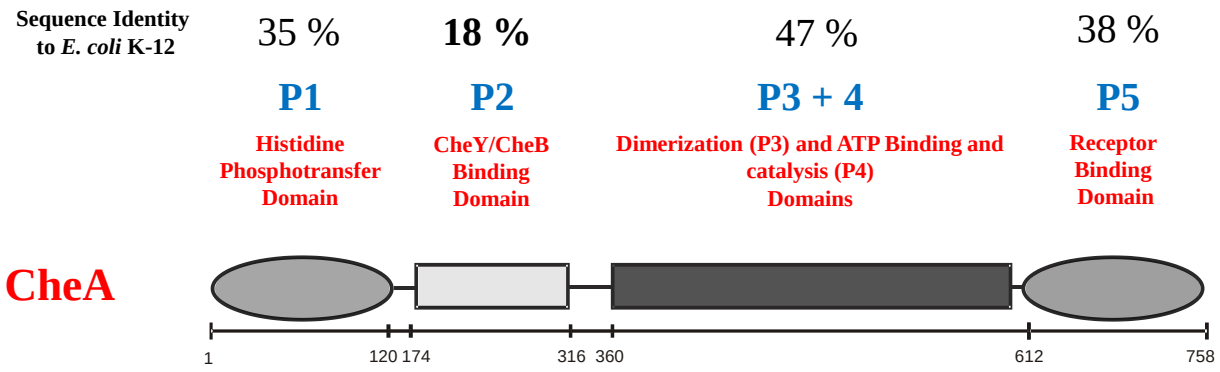

Figure 2.5. Domain structure of *S. meliloti* CheA. P1, phosphotransfer; P2, ligand binding; P3, dimerization; P4, catalytic; P5, receptor coupling and sensor. Numbers below refer to amino acid residues at domain boundaries.

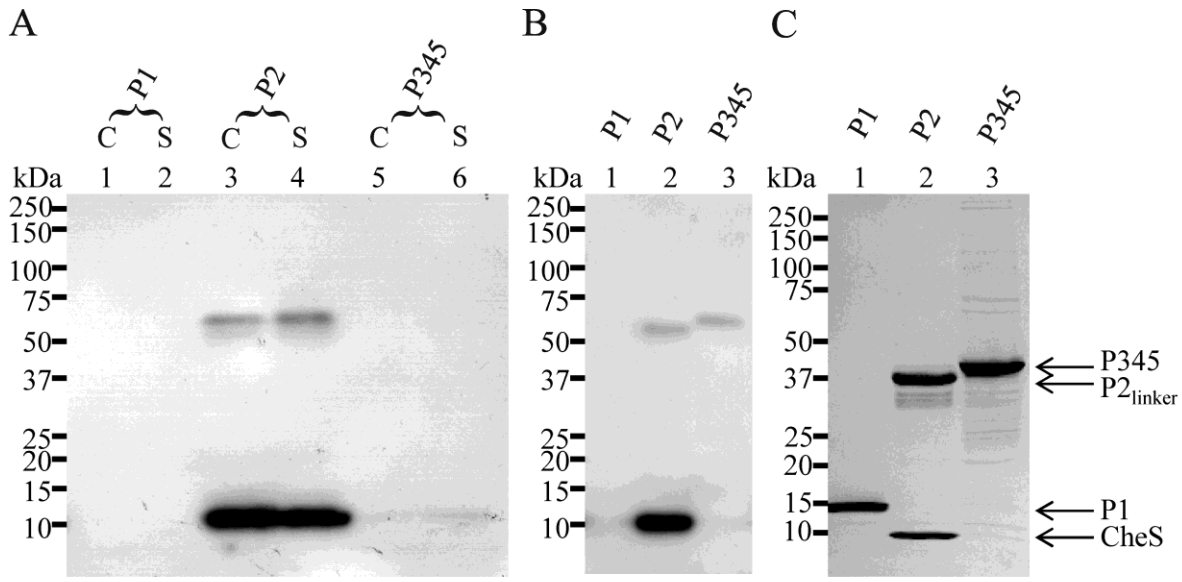

Figure 2.6. SDS-PAGE and immunoblots to assess co-expression and purification of CheS and His_6-CheA domains. **A.** Equal volumes of cell extracts and soluble fractions were separated on a 10-20% SDS-gel, transferred onto a PVDF membrane and probed with anti-CheS antibody. Lanes 1 and 2: Whole cell extract (C) and soluble fraction (S) of *E. coli* BL21DE3 (pBS1007) expressing CheS and His_6-P1 (1-135 aa); Lanes 3 and 4: whole cell extract (C) and soluble fraction (S) of *E. coli* BL21DE3 (pBS330) expressing CheS and His_6-$P2_{linker}$ (aa 120-360); Lanes 5+6: whole cell extract (C) and soluble fraction (S) of *E. coli* BL21DE3 (pBS339) expressing CheS and His_6-P345 (355-758 aa). **B** and **C.** Proteins after chromatography on Ni-NTA Sepharose were separated on a 10-20% SDS-gel, and **B.** transferred onto PDVF membrane and probed with anti-CheS antibody; or **C.** stained with Coomassie brilliant blue. Lane 1: P1/CheS (expressed from pBS1007); lane 2: CheA-$P2_{linker}$/CheS (expressed from pBS317); lane 3: P345/CheS (expressed from pBS339).

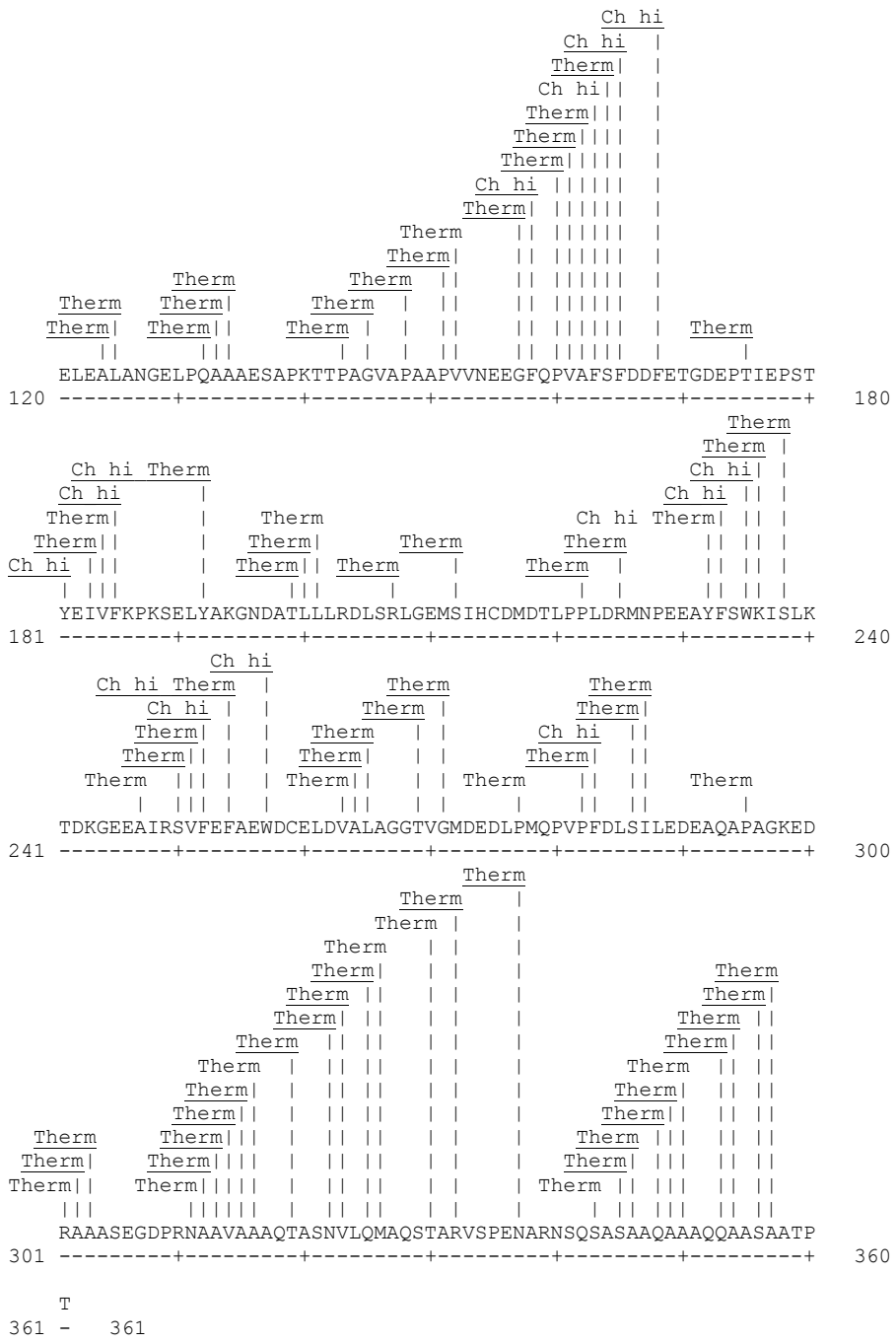

Figure 2.7. Predicted cleavage sites of proteolytic enzymes in $P2_{linker}$. Chymotrypsin (high-specificity), indicated as Ch_hi and Thermolysin, indicated as Therm cleavage sites on the His_6-$P2_{linker}$ amino acid sequence. The proteolytic map was derived from the PeptideCutter program on EXPASY (102).

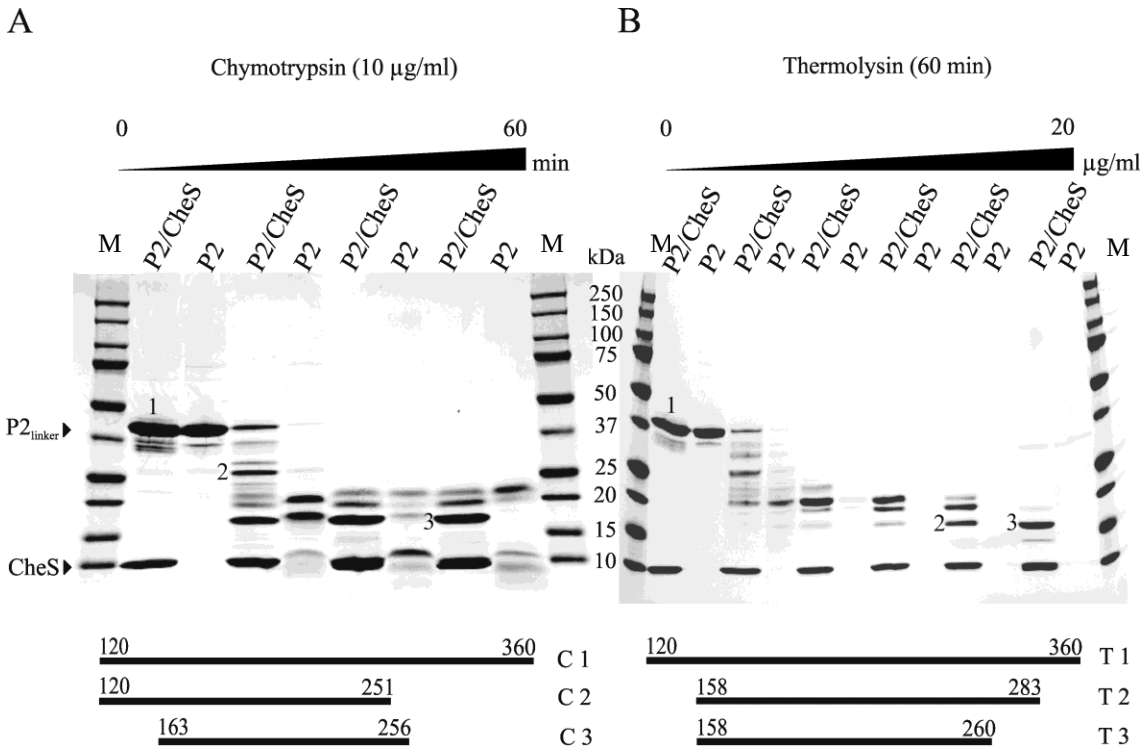

C

```
121                                                                 180
E LEALANGELP QAAAESAPKT TPAGVAPAAP VVNEEGFQPV AFSFDDFETG DEPTIEPSTY
181                                                                 240
EIVFKPKSEL YAKGNDATLL LRDLSRLGEM SIHCDMDTLP PLDRMNPEEA YFSWKISLKT
241                                                                 300
DKGEEAIRSV FEFAEWDCEL DVALAGGTVG MDEDLPMQPV PFDLSILEDEA QAPAGKEDR
301                                                                 360
AAASEGDPRN AAVAAAQTAS NVLQMAQSTA RVSPENARNS QSASAAQAAAQ QAASAATPT
```

Figure 2.8. Time course of limited proteolysis of the His_6-$P2_{linker}$/CheS complex as determined by SDS-PAGE and identified fragments. **A.** Proteolysis by chymotrypsin, and **B.** Proteolysis by thermolysin. Samples from the His_6-$P2_{linker}$/CheS and His_6-$P2_{linker}$ digestions were loaded in odd and even numbered lanes, respectively. Arrows indicate the positions of CheA-P2 and CheS, molecular markers are shown in the center. Numbers indicate the positions of proteolytic products on the SDS-gels which are shown in the panels below. **A.** Digestions were performed at final concentrations of chymotrypsin of 10µg/ml. Aliquots were withdrawn at 5, 20, 40, and 60 min and reactions were stopped by the addition of SDS-gel loading buffer. **B.** Digestions were performed at final thermolysin concentrations of 0.08µg/ml, 0.4µg/ml, 1.2µg/ml, 5µg/ml, 20µg/ml for 60 min at 37 °C. Reactions were stopped by the addition of EDTA and SDS-gel loading buffer. **C.** Amino acid sequence of the $P2_{linker}$ domain. The region protected by CheS is shaded dark grey (core domain, as determined after chymotrypsin digestion) and light grey (additional residues, as determined after thermolysin digestion). The area protected by CheY2 according to Riepl *et al.* (66) is marked by a black line.

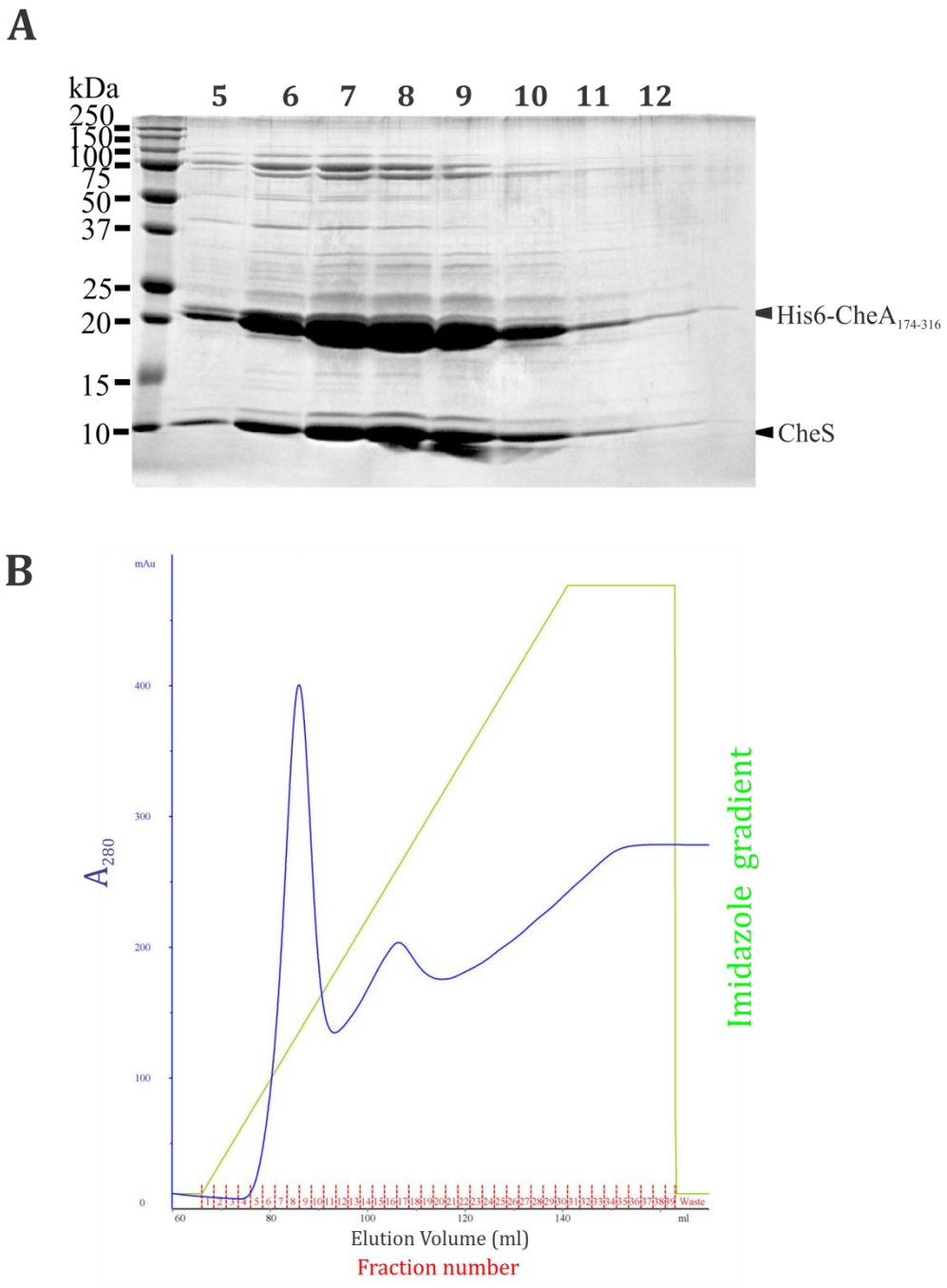

Figure 2.9. Co-expression and -purification of His_6-$CheA_{174-316}$/CheS. The protein complex was expressed in *E. coli* BL21DE3 cells and the lysate was purified by Ni-NTA affinity chromatography as described in methods. A. Fractions containing protein were electrophoretically separated in a 15% (w/v) acrylamide gel containing SDS. M indicates the molecular weight marker, numbers 5-12 indicate fraction numbers. B. Elution profile obtained during Ni-NTA affinity purification process, with the A_{280} peak of the protein in blue, the gradient of imidazole in green and fractions marked in red on the X axis.

Chapter 3

Analysis of the role of CheS in phosphotransfer in *Sinorhizobium meliloti* chemotaxis

Abstract

The phenotype of the *cheS* deletion mutant indicates the participation of CheS in modulating phosphate flow in *S. meliloti* chemotaxis by possibly regulating the intracellular concentration of CheY2~P. To investigate this possibility, the role of CheS in autophosphorylation of CheA, dephosphorylation of CheY1~P and CheY2~P, and in retrophosphorylation of CheY2~P to CheA was studied. Although CheS binds to CheA, it does not affect the rate of autophosphorylation of CheA in the presence of [γ-^{32}P]ATP. Furthermore, CheS does not affect the rate of [^{32}P]phospho-CheY2 dephosphorylation. However, CheS increases the rate of [^{32}P]phospho-CheY1 dephosphorylation two-fold. In retrophosphorylation reactions involving CheY1 and CheY2 phosphorylated by acetyl [^{32}P]phosphate, earlier observations that [^{32}P]phospho-CheY2 can transfer its phosphate to CheA, while [^{32}P]phospho-CheY1 cannot, were confirmed. CheS does not seem to affect the retrophosphorylation reaction from [^{32}P]phospho-CheY2 alone, or in the presence of [^{32}P]phospho-CheY1 to CheA. The phenotype of the Δ*cheS* strain might be explained by the two-fold increase in CheY1 dephosphorylation. The exact mechanism of this action is not known at this time and further studies are needed.

Materials and methods

Expression and purification of response regulators

His_6-CheA, His_6-CheA/CheS were expressed in *E. coli* BL21DE3. The proteins were purified using Ni-NTA affinity chromatography as described in Chapter 2, except, the binding and elution buffers contained 20% glycerol. CheY1 and CheY2 proteins were expressed from derivatives of the pTYB1 plasmid (Table 2.1), which added an N-terminal chitin-binding domain (CBD) and self-cleavable intein tag to the protein. These proteins were expressed in *E. coli* ER2566 as described earlier and purified by IMPACT chromatography. Intein mediated cleavage at the intein-cleavage site was initiated by incubating the chitin beads with IMPACT buffer containing 50mM dithiothreitol (DTT) for 16 hours at 4°C. His_6-CheA, His_6-CheA/CheS, CheY1 and CheY2 eluant fractions were analyzed on 15% (w/v) SDS-acrylamide gels, and protein containing fractions were pooled and concentrated using an Amicon concentration cell with the appropriate cutoff membrane filters. Next, they were subjected to size exclusion chromatography and buffer exchange on a SR-300 gel filtration column with $TEDG_{10}$ (50 mM Tris-HCl, pH 8.0, 1 mM EDTA, 1 mM DTT, 10% glycerol) buffer at a flow rate of 0.5ml/minute. The fractions containing protein were separated on a 15% (w/v) SDS-acrylamide gel and fractions containing pure protein were pooled and concentrated with the Amicon concentration cell. The concentrated pool was filtered through a 0.2 μm low protein binding cellulose acetate syringe filter, and the protein concentration was determined by the Bradford assay, using known concentrations of bovine serum albumin (BSA) as reference standards. The protein solutions were aliquoted, flash frozen in liquid nitrogen, and stored at -80°C till further use in the assays. CheB protein had been purified by Hardik Zatakia in 2009 and stored at -80°C. An aliquot of CheB

was subjected to buffer exchange by dialysis against $TEDG_{10}$ buffer, protein concentration was determined, and the protein was stored frozen at -20°C till use in the assays.

Autophosphorylation of CheA and CheA/CheS

The autophosphorylation kinetics of CheA and CheA/CheS were determined according to the procedures described by Sourjik and Schmitt (84). All phosphorylation reactions were performed in freshly prepared $TEDG_{10}$ buffer, pH 8.0, and were supplemented with 5mM $MgCl_2$ and 50mM KCl. Reactions were performed at room temperature (~22°C). The final concentration of His_6-CheA and His_6-CheA/CheS in the reaction mixture was 2μM in the initial autophosphorylation reactions and varied between 2 and 10μM in the reactions to determine the phosphorylation state of CheA and CheA/CheS. Reaction times are specified in the figure legends (Figure 3.1). Autophosphorylation of CheA and CheA/CheS was initiated by the addition of [γ-^{32}P]ATP equivalent to 3μCi activity and 0.4mM concentration in a 200μl volume. Phosphorylation was measured by sampling 10μl aliquots of the reaction mixture at given intervals and stopping the reaction by addition of 10μl of 6X-SDS-PAGE gel loading buffer containing 10mM EDTA. Samples were separated by electrophoresis on a 4-20% gradient Criterion SDS-PAGE gel (Bio-Rad). Immediately following electrophoresis, the gels were enclosed in plastic cling-film and exposed on a storage phosphor screen (GE Life Sciences) which had been erased earlier by exposure to a 500 W photoflood tungsten light bulb with a yellow filter (Wratten 16). Following autoradiography, the phosphor screen was excited using a red (633nm) excitation LASER on the Typhoon Trio Phosphorimager (GE Healthcare) and observed using a 390nm Band-pass filter. Band intensity was quantified by the ImageQuant™ TL (GE Healthcare) software. The kinetic time courses were plotted using the Origin 8.1 (Origin Lab) software.

Preparation and purification of [^{32}P]phospho-CheA and [^{32}P]phospho-CheA/CheS

500µg His_6-CheA and His_6-CheA/CheS were phosphorylated using [γ-^{32}P]ATP equivalent to 100µCi activity and 0.4mM concentration in a 500µl final volume of $TEDG_{10}$ supplemented with 5mM $MgCl_2$ and 50mM KCl as described above. The reactions were performed at room temperature (~22°C). Briefly, 100µCi of [γ-^{32}P]ATP to a final concentration of 0.4mM was added to the reaction mixture containing CheA or CheA/CheS, 5mM $MgCl_2$, 50mM KCl and $TEDG_{10}$ and the reaction was allowed to proceed for 2 minutes. Unlabeled ATP in $TEDG_{10}$ buffer was then added to a final concentration of 0.4mM in the reaction and incubated to a total of 15 minutes. The reaction mixture was then subjected to size exclusion chromatography on a SR25/45 (GE Healthcare) gel filtration column containing Sephadex G-50 (GE Healthcare) with a bed height of 40ml that was equilibrated and developed with $TEDG_{10}$ to purify [^{32}P]phospho-CheA or [^{32}P]phospho-CheA/CheS from [γ-^{32}P]ATP + ADP and ^{32}Phosphate at a flow rate of 0.5ml/minute. Fractions were collected using a FRAC-100 fraction collector (Pharmacia), and the phosphorylated protein containing fractions were identified by liquid scintillation counting on the LS6500 Liquid Scintillation counter (Beckman-coulter). Fractions containing the phosphorylated protein were pooled, aliquoted into 1.5ml reaction tubes and immediately placed in a -20°C freezer. The concentration of phosphorylated proteins was determined by the Bradford assay and specific activities of the phosphorylated proteins were determined by liquid scintillation counting. Proteins were stored at -20°C till further use.

Dephosphorylation kinetics of CheY1 and CheY2

Phosphotransfer reactions from purified [^{32}P]-CheA or [^{32}P]-CheA/CheS were initiated by the addition of CheY1 or CheY2 to the reaction. [^{32}P]-CheA or [^{32}P]-CheA/CheS were present in a 10-fold molar excess to CheY1 or CheY2, namely, the 250µl reactions contained 107pmol CheA or CheA/CheS and 10.7pmol CheY1 or CheY2. The reaction mixture contained 5mM $MgCl_2$ and made up to volume with $TEDG_{10}$. 20µl of [^{32}P]-CheA or [^{32}P]-CheA/CheS were withdrawn from the reaction mixture and added to 10µl of 6X- SDS-PAGE gel loading buffer containing 10mM EDTA, before the addition of CheY1 or CheY2, serving as controls. 1µl of CheY1 or CheY2 mixtures containing 7.5mM BSA (New England Biolabs) and 5mM $MgCl_2$ in $TEDG_{10}$ buffer were then added to the reaction, 20µl aliquots were withdrawn at fixed intervals, and added to 10µl of 6X- SDS-PAGE gel loading buffer containing 10mM EDTA to stop the phosphotransfer reaction. The samples were subjected to electrophoresis and autoradiography as described above. Kinetic time courses were plotted using Origin 8.1 software.

Preparation and assay of acetyl [^{32}P]phosphate

Acetyl [^{32}P]phosphate was prepared according to the protocol described by Stadtman (86) with modifications to the protocol as described by McCleary and Stock (46). Briefly, 240µl of pyridine, 63µl of 2M K_2HPO_4 and [^{32}P]carrier-free orthophosphate (Perkin-Elmer, NEX053-H) equivalent to 1.5mCi of activity were added to an ice-cold 5ml (18mm diameter) glass tube containing a magnetic stir-bar, and the volume of the reaction was made up to 740µl with H_2O. This mixture was stirred on ice for 5min, and adequate mixing was ensured. 27.5µl of chilled acetic anhydride was added drop by drop to the reaction mixture in one minute time intervals. After the addition of the last drop, the mixture was

allowed to stir on ice for 2 minutes. 216µl of freshly prepared 2N LiOH solution was slowly added to the mixture, and allowed to stir on ice for 3 minutes. 246µl aliquots of the reaction mixture were transferred to cold 2ml reaction tubes, and 1.44ml of chilled ethanol was added drop by drop to precipitate acetyl [^{32}P]phosphate. The mixture was briefly vortexed to allow the complete mixing of the reaction mixture and allowed to incubate on ice for 1 hour. The precipitate was separated by centrifugation at 11,200 g for 15 minutes at 4°C in a pre-cooled refrigerated centrifuge (Eppendorf). The supernatant was carefully pipetted out and discarded, the resultant pellet was resuspended in 1.44ml cold ethanol, and centrifuged for 15 min. This washing step was performed three times. Finally, the pellet was allowed to air dry for 15 min and placed inside a vacuum desiccator for 2-3 days at 4°C for drying. The pellet was dissolved in 400µl of H_2O and aliquoted 20µl per 1.5ml reaction tube. The resultant solution was clear with very little suspended particulate matter. The concentration of acetyl [^{32}P]phosphate was determined by a modification of the procedure described by Lipmann and Tuttle (39). Standard solutions of acetohydroxamic acid were prepared in water. 400µl of the standard solution from 0 to 1mM acetohydroxamic acid in a 1.2ml volume, or 0.5% acetyl [^{32}P]phosphate solution in water was added to a 1.5ml reaction tube. 200µl of neutralized hydroxylamine solution containing equal volumes of 28% (w/v) solution of $NH_2OH.HCl$ and 14% (w/v) NaOH solution were added to the tube and allowed to react for 10 minutes at room temperature. After incubation, 600µl of ferric chloride solution containing equal volumes of 5% (w/v) $FeCl_3$ (in 0.1N HCl), 12% (w/v) tri-chloro acetic acid and 3N HCl were added to the mixture. After color development in 30s, the absorbance of the solution was determined at 540nm. The concentration of acetyl

[^{32}P]phosphate was determined by comparing the absorbance to a standard curve of the A_{540} of the acetohydroxamic acid standards.

Retrophosphorylation assays

The phosphorylation of 5μM CheY1 and CheY2 was initiated by the addition of 18mM acetyl [^{32}P]phosphate to the reaction mixture containing 5mM $MgCl_2$, 50mM KCl and $TEDG_{10}$ in a final volume of 20μl, following the procedure described by Sourjik and Schmitt (84). 5μM CheA or CheA/CheS that were adjusted to the same buffer conditions were added to the reaction mixture. For the control mix $TEDG_{10}$ containing 5mM $MgCl_2$ and 50mM KCl was added instead of CheA or CheA/CheS. After initiation of CheY1 and CheY2 phosphorylation with acetyl [^{32}P]phosphate, the reaction was allowed to proceed for 60s, after which, the mixture containing CheA, CheA/CheS or $TEDG_{10}$ was added to the phosphorylation reaction, and allowed to incubate for 20 seconds. The reaction was stopped by the addition of 10μl of 6X gel-loading buffer containing 10mM EDTA. Samples were subjected to electrophoresis and autoradiography as described above. After electrophoresis, the portion of the gel containing the dye-front and excessive acetyl [^{32}P]phosphate and [^{32}P]phosphate was excised with a clean blade, since the activity from the acetyl [^{32}P]phosphate trapped in the dye front would overlap the activity from [^{32}P]phospho CheY1 or [^{32}P]phospho CheY2.

Results and discussion

CheS does not affect CheA autophosphorylation

To determine the effect of CheS on CheA autophosphorylation, recombinant His_6-CheA or His_6-CheA/CheS (2μM) were incubated with [γ-^{32}P]ATP. Aliquots were removed at specified intervals, the reaction was terminated by addition to 6X-SDS-PAGE sample loading buffer containing 10mM EDTA, and separation was carried out by SDS-PAGE. Post autoradiography (Figure 3.1), the band intensities of [^{32}P]phospho-CheA and [^{32}P]phospho-CheA/CheS were determined by excitation of the storage phosphor screen in the Typhoon Trio phosphorimager. The time course of CheA or CheA/CheS phosphorylation by [γ-^{32}P]ATP was plotted, with the peak-volume data from all the time points was normalized to the band intensity of [^{32}P]phospho-CheA or [^{32}P]phospho-CheA/CheS at saturation. This peak volume data point (15min) was designated as [^{32}P]-$CheA_{final}$ or [^{32}P]-$CheA_{final}$/CheS. The phosphorylation data was collated in Microsoft Excel 2010, and the resulting data was plotted using the Origin 8.1 software (Figure 3.2). The lines through the experimental data sets represent least-squares fits of the data to single-exponential curves. The phosphorylation of CheA at a saturating ATP concentration follows a simple exponential time course, with the reaction reaching V_{max} at 3min after the addition of [γ-^{32}P]ATP. The half-time ($t_{1/2}$) value for the reaction was 45sec. Phosphorylation of CheA/CheS also followed a simple exponential time course, with the $t_{1/2}$ value for the reaction being 45sec, like the $t_{1/2}$ value of CheA autophosphorylation. The data indicates that CheS does not influence the autophosphorylation of CheA.

CheS accelerates CheY1 dephosphorylation but does not affect the dephosphorylation rates of CheY2 or CheB

The swimming phenotype of the *S. meliloti* Δ*cheS* mutant strain was similar to the phenotype of the Δ*cheY1* mutant. Both mutants exhibited a slower swimming speed which indicated that the cellular level of CheY2~P in both strains was higher than in the wild-type strain. Since CheY1 participates in signal termination by acting as a phosphate sink for the phosphate groups released from CheY2 via CheA, it is possible that CheS participates in this reaction. A possible mechanism for signal termination by CheS is an increased dephosphorylation rate of CheY1 or CheY2. If CheS accelerates the spontaneous dephosphorylation rate of CheY2~P, the intracellular concentration of CheY2~P would decrease leading to a lower rate of tumbles and increased swimming speed as seen in the *cheS* deletion mutant. If CheS accelerates the dephosphorylation of CheY1, it would shift the CheY2~P – CheA~P – CheY1~P equilibrium to the right, thus accelerating the CheA-dependent withdrawal of phosphate from CheY2. This would result in faster signal termination and would explain the phenotype of the Δ*cheS* mutant. To verify this hypothesis, an experiment was performed to determine the rate of CheY2 dephosphorylation in the presence and absence of CheS. CheA and CheA/CheS had been phosphorylated with [γ-^{32}P]ATP and the resulting phosphorylated proteins were separated from free [^{32}P]-ATP, ADP and [^{32}P]phosphate by size exclusion chromatography. The specific activity of [^{32}P]phospho-CheA was 0.2Ci/mole and that of [^{32}P]phospho-CheA/CheS was 0.3Ci/mole. 107pmoles of purified, phosphorylated CheA or CheA/CheS were added to the reaction in which these proteins were at a 10-fold molar excess over CheY2 (10.7 pmoles). Since CheA is in a 10-fold molar excess over CheY2 in the reaction and the

dephosphorylation rate of CheY2~P is slower than that of the phosphate transfer rate from CheA~P to CheY2, the dephosphorylation of CheY2~P is the rate-limiting step in the reaction. Initially, 20µl of the CheA or CheA/CheS mixture containing 50mM KCl and 5mM $MgCl_2$ were withdrawn as a control. CheY2 mixture containing 5mM $MgCl_2$ and 7.5mM BSA (to stabilize CheY2 at high dilution) was added to the reaction to initiate phosphotransfer and aliquots were withdrawn from the mixture at specific time intervals. All peak volume data points obtained from the autoradiograms (Figure 3.5) were normalized against the control [^{32}P]phosho-CheA$_{total}$ time point using MicroSoft Excel 2010 software, and the resultant data was plotted using Origin 8.1. Under the given experimental conditions, [^{32}P]phospho-CheA decayed with a $t_{1/2}$ of 47sec and [^{32}P]phospho-CheA/CheS decayed with a $t_{1/2}$ of approximately 45sec in the presence of CheY2 (Figure 3.6). Hence, CheS does not affect CheY2 dephosphorylation rate.

A similar experiment was performed to determine the dephosphorylation rate of CheY1 in the presence and absence of CheS. From plotted data obtained from the autoradiograms (Figure 3.3), it was observed that [^{32}P]phospho-CheA decayed with a $t_{1/2}$ of 40sec and [^{32}P]phospho-CheA/CheS decayed with a $t_{1/2}$ of approximately 25sec in the presence of CheY1 (Figure 3.4). The presence of CheS accelerated the transfer of [^{32}P]phosphate from CheA to CheY1 almost by a factor of 2, which indicates a faster rate of dephosphorylation of [^{32}P]phospho-CheY1. The effect of CheS on the dephosphorylation of CheB was also observed (Figure 3.7). CheB is a third response regulator phosphorylated by CheA, which is involved in adaptation. Due to its low concentration in the cell, it is not anticipated to act as a phosphate sink (38). However, for comparison CheB was included in the experiment. CheS did not affect the dephosphorylation rates of CheB as evident from the decay rates of

[^{32}P]-CheA or [^{32}P]-CheA/CheS. A [^{32}P]phospho-CheB band was not observed in the autoradiograms (Figure 3.8). This could have been due to the fast dephosphorylation of CheB in the reaction mixture (95). This could also mean that the dephosphorylation of CheB in this reaction is not rate-limiting.

To establish that the decay of [^{32}P]phospho-CheA or CheA/CheS was indeed due to the transfer of phosphate to CheY1, CheY2 or CheB, two control experiments were performed in the absence of a response regulator as described above. 30% phosphate was lost from both CheA and CheA/CheS in the first three time points and then the phosphate groups on appeared to be stable (Figures 3.9 and 3.10). However, the reason for the observed loss of phosphate in the initial time points can only be speculated on. Since [^{32}P]-CheA and [^{32}P]-CheA/CheS were pre-incubated for the phosphotransfer experiments, the initial loss of phosphate groups were not observed in these experiments.

The role of CheS in retrophosphorylation

In addition to phosphorylation by their cognate kinases, response regulators can be phosphorylated by small phosphodonors such as acetyl phosphate (46). The retrophosphorylation event from acetyl [^{32}P]phosphate activated phospho-CheY2 to CheA has been demonstrated by Sourjik and Schmitt (84). The same [^{32}P]phosphate group is then transferred from phospho-CheA to CheY1. Acetyl [^{32}P]phosphate activated CheY1, however, cannot transfer the phosphate group to CheA. Therefore, this technique can be used to study the retrophosphorylation event and the role of CheS. In a control experiment, saturated levels of [^{32}P]phospho-CheY1 or CheY2 were reached in 60sec after the addition of acetyl [^{32}P]phosphate (data not shown), in agreement with Sourjik and Schmitt (84).

Also, the [^{32}P]phosphate group was transferred from [^{32}P]-CheY2 to CheA within 20sec in control time-course reactions (data not shown). Three controls were prepared for each set, containing 5μM CheY1, CheY2 or CheY1 + CheY2. These controls were phosphorylated by the addition of 18mM acetyl [^{32}P]phosphate and the reaction was allowed to proceed for 60sec. Then $TEDG_{10}$, CheA, or CheA/CheS were added to the mixture for 20sec and the reaction was stopped by the addition of 10μl of 6X gel-loading buffer containing 10mM EDTA. Samples were separated by electrophoresis as described and intensities from their autoradiograms were compared to determine the relative phosphorylation states of CheY1 and CheY2 (Figure 3.11). Notably, SDS-PAGE gels were exposed on the storage phosphor screen for up to 50h to obtain sufficient signal for analysis. The resulting autoradiogram shows the phosphorylation of CheY1 and CheY2 by acetyl [^{32}P]phosphate (Figure 3.11, lanes 1, 2 and 3). [^{32}P]-CheY1 fails to retro-transfer its phosphate to CheA, in the presence or absence of CheS (84) (Figure 3.11, lanes 4 and 5). [^{32}P]-CheY2 transfers its phosphate to CheA, though phosphorylated CheA was not visible in the autoradiograms and this transfer is not affected by the presence of CheS (Figure 3.11, lanes 6 and 7). A stronger indication of this event was obtained in a similar experiment, where the CheY2~P bands in the presence of CheA or CheA/CheS were weaker (Figure 3.12, lanes 5 and 9) than in the absence of CheA or CheA/CheS (Figure 3.12, lane 2). However, the data from retrophosphorylation assays indicates that CheS does not play a role in the retrotransfer of phosphate groups from CheY2~P to CheA.

Conclusions

The possibility that CheS regulates phosphate flow in the chemotaxis signaling chain of *S. meliloti* was investigated. Following experimental conditions described by Sourjik and Schmitt (84), three types of experiments were performed. To analyze if CheS influenced the autophosphorylation of CheA, CheA or the CheA/CheS complex was phosphorylated in the presence of 0.4mM [γ-^{32}P]ATP containing 3μCi activity. The resultant data indicates that CheA autophopsphorylation proceeds in a simple exponential time course, reaching saturation at 15 minutes. However, CheS does not influence the autophosphorylation of CheA. To determine the role of CheS in the dephosphorylation of the response regulators in the chemotaxis chain, CheY1, CheY2, or CheB were added to purified [^{32}P]phospho-CheA or [^{32}P]phospho-CheA/CheS in a 1:10 molar ratio. The resulting time course of [^{32}P]phospho-CheA decay in the presence of the response regulator and the presence of absence of CheS indicates that, while CheS does not influence the dephosphorylation of CheY2 or CheB, it increases the rate of CheY1 dephosphorylation two-fold. The mechanism by which CheS increases CheY1 dephosphorylation, by directly interacting with CheY1~P or through interaction in the CheA/CheS/CheY1 complex is not known. Finally, the role of CheS in the retro-phosphorylation events was analyzed by phosphorylation of CheY1 or CheY2 with acetyl [^{32}P]phosphate, and the subsequent addition of CheA or the CheA/CheS complex. While CheY1 or CheY2 are successfully phosphorylated, and CheY2 transfers its phosphate to CheA, CheS did not seem to influence the retrophosphorylation events.

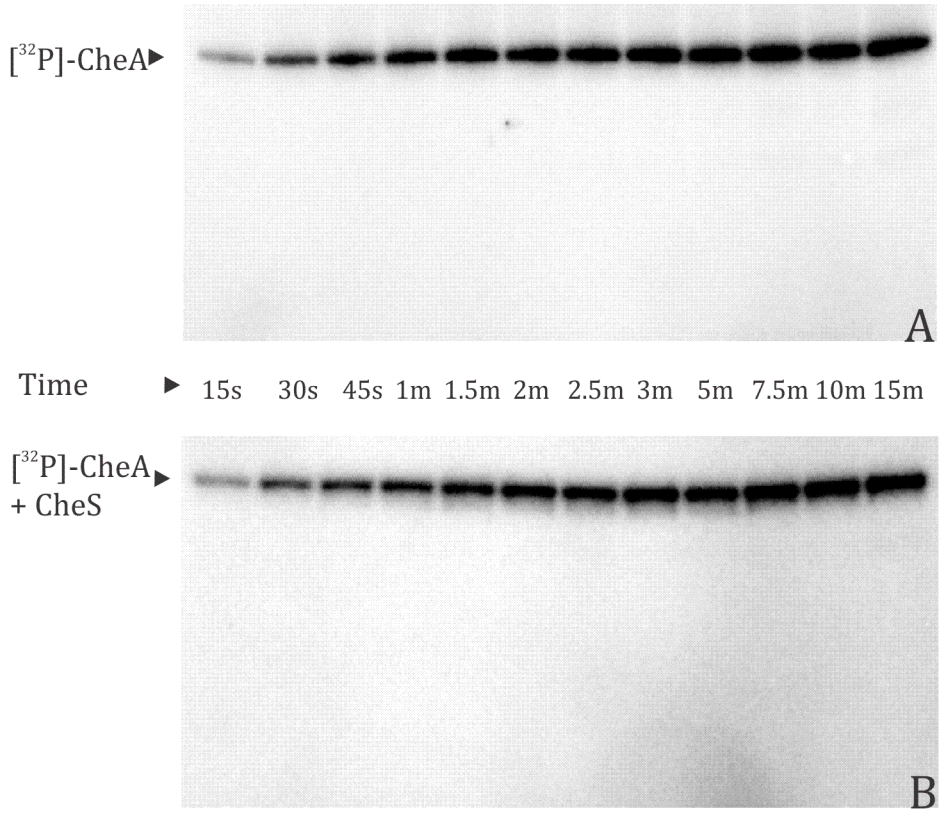

Figure 3.1. Autoradiogram showing the autophosphorylation of CheA and CheA/CheS. CheA or CheA/CheS (2μM) was incubated with 0.4mM [γ-^{32}P]ATP at room temperature. Aliquots (10μl) were withdrawn at specified intervals, and the reaction was terminated by the addition of 10μl of 6X gel-loading buffer containing SDS and 10mM EDTA. After separation of the samples by SDS-PAGE, gels were exposed to a storage phosphor screen, and the resultant image is shown above. (A) Autoradiogram of CheA autophosphorylation and (B) of CheA/CheS autophosphorylation.

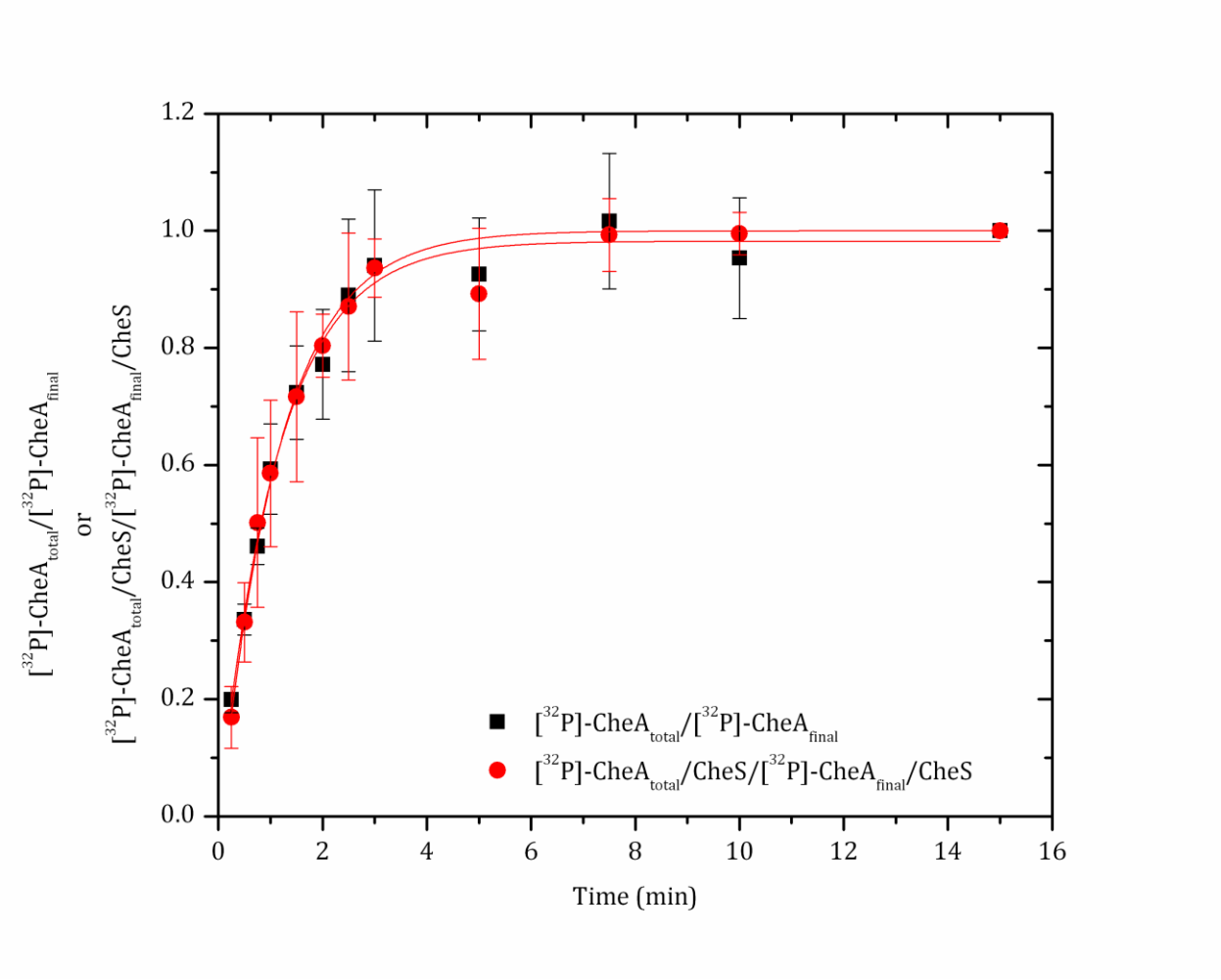

Figure 3.2. Time course of CheA and CheA/CheS autophosphorylation. All data points were normalized to the band intensity of the 15min timepoint. CheA data points are indicated by black closed squares and CheA/CheS data points are indicated by red closed circles. Each data point represents the average from three experiments. Black and red lines represent a computer-generated least-squares fit to a single exponential curve using the Origin 8.1 program.

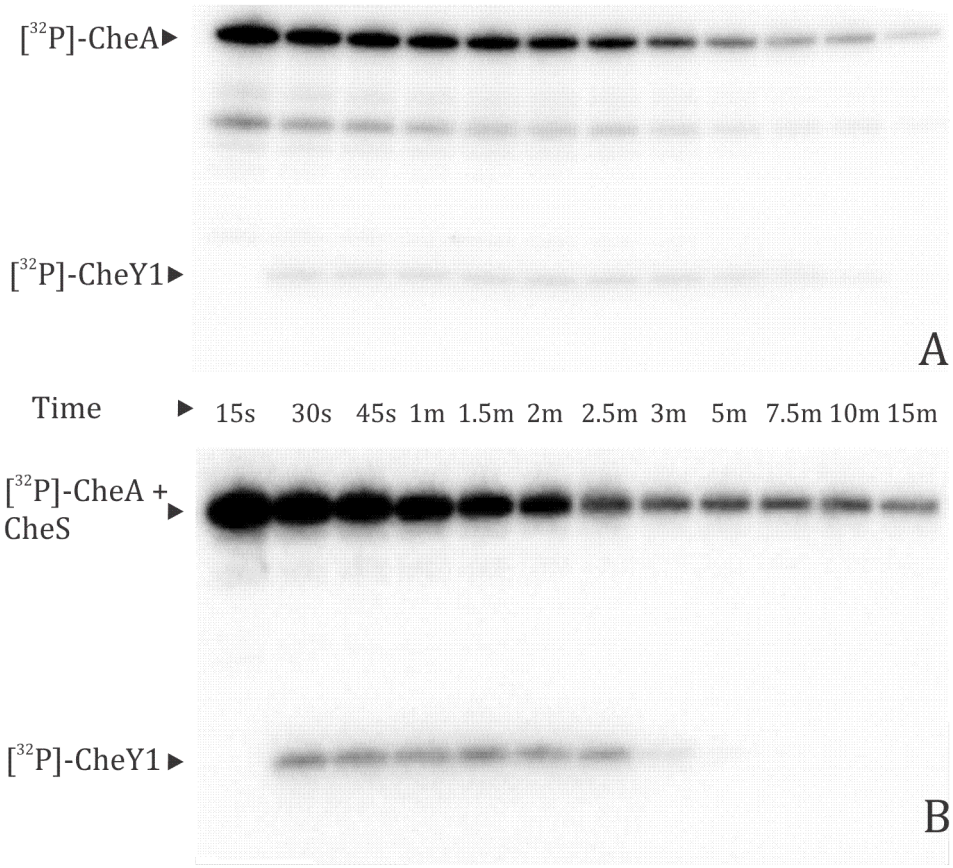

Figure 3.3. Autoradiogram showing dephosphorylation of CheY1 following phosphotransfer from [^{32}P]phospho-CheA or CheA/CheS. A 10-fold molar excess of [^{32}P]-CheA or [^{32}P]-CheA/CheS was incubated CheY1 at room temperature. Aliquots (20µl) were withdrawn at specified intervals, and the reaction was terminated by the addition of 10µl of 6X gel-loading buffer containing 10mM EDTA. A 20µl aliquot of [^{32}P]-CheA or [^{32}P]-CheA/CheS was withdrawn before CheY1 addition and served as the control (C). After separation of the samples by SDS-PAGE, gels were exposed to a storage phosphor screen and the resultant image is shown above. (A) [^{32}P]-CheA and (B) [^{32}P]-CheA/CheS with CheY1.

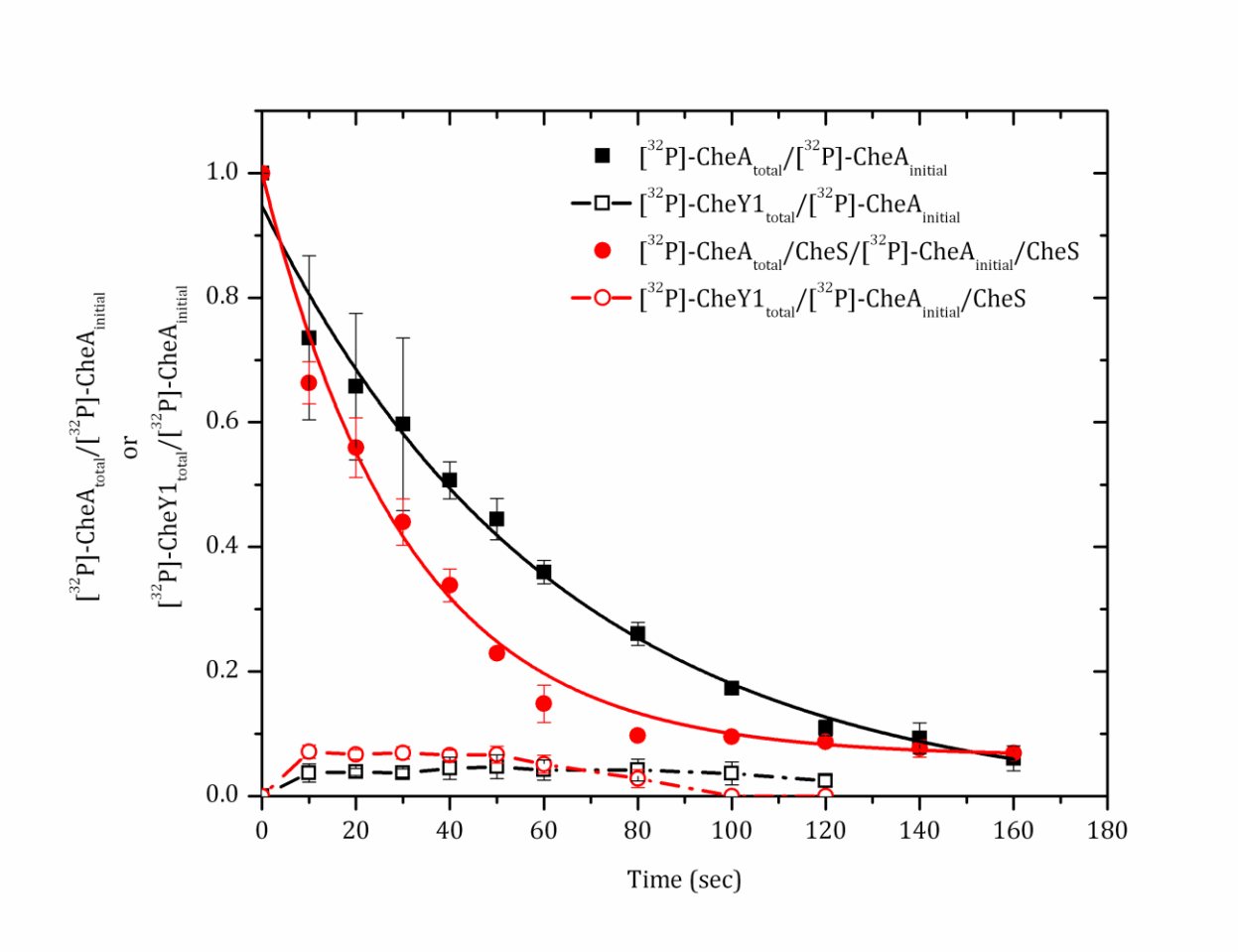

Figure 3.4. Time course of CheY1 dephosphorylation in the presence of CheA and CheA/CheS. All data points from three independent experiments, including [^{32}P]-CheA and [^{32}P]-CheY1 are normalized against the control sample of [^{32}P]-CheA taken before the addition of CheY1. [^{32}P]-CheA data points are represented as solid black squares and [^{32}P]-CheA/CheS data points as solid red circles. [^{32}P]-CheY1 data points in the presence of CheA are represented as open black squares and those in the presence of CheA/CheS are represented as open red circles. Black and red lines represent computer-generated least squares fits of the data to single exponential decay curves using Origin 8.1.

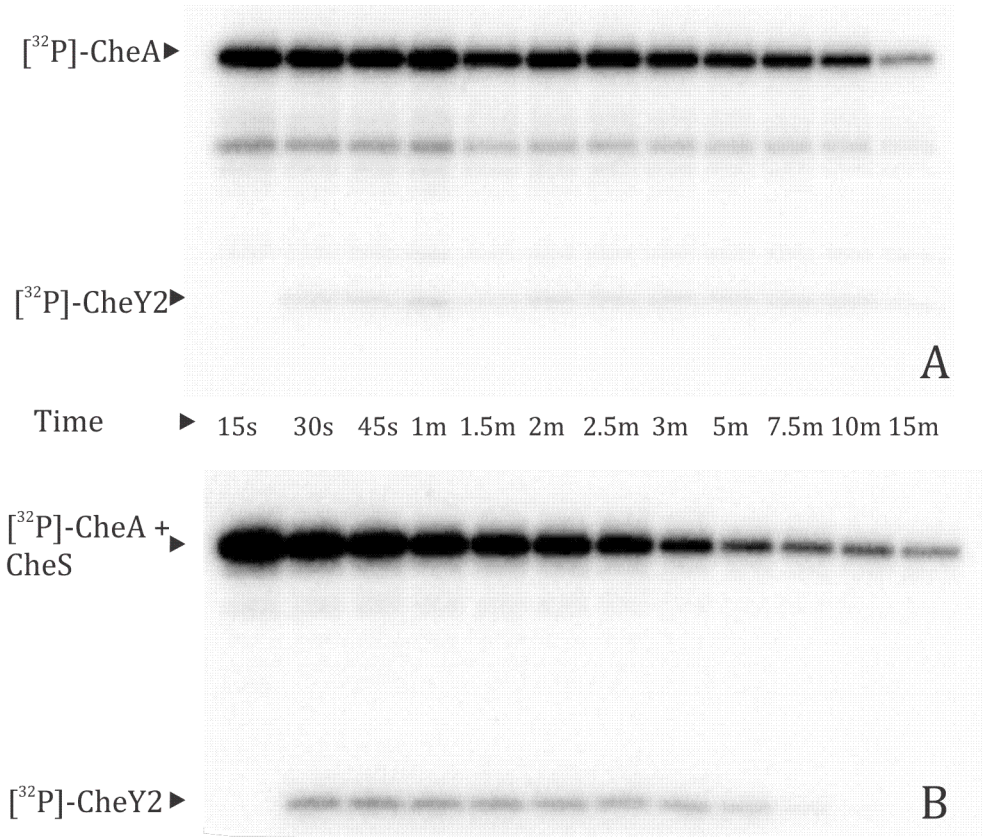

Figure 3.5. Autoradiogram showing dephosphorylation of CheY2 following phosphotransfer from [^{32}P]phospho-CheA or CheA/CheS. A 10-fold molar excess of [^{32}P]-CheA or [^{32}P]-CheA/CheS was incubated with CheY2 at room temperature. Aliquots (20µl) were withdrawn at specified intervals, and the reaction was terminated by the addition of 10µl of 6X gel-loading buffer containing 10mM EDTA. A 20µl aliquot of [^{32}P]-CheA or [^{32}P]-CheA/CheS was withdrawn before CheY2 addition and served as the control (C). After separation of the samples by SDS-PAGE, gels were exposed to a storage phosphor screen, and the resultant image is shown above. (A) [^{32}P]-CheA and (B) [^{32}P]-CheA/CheS with CheY2.

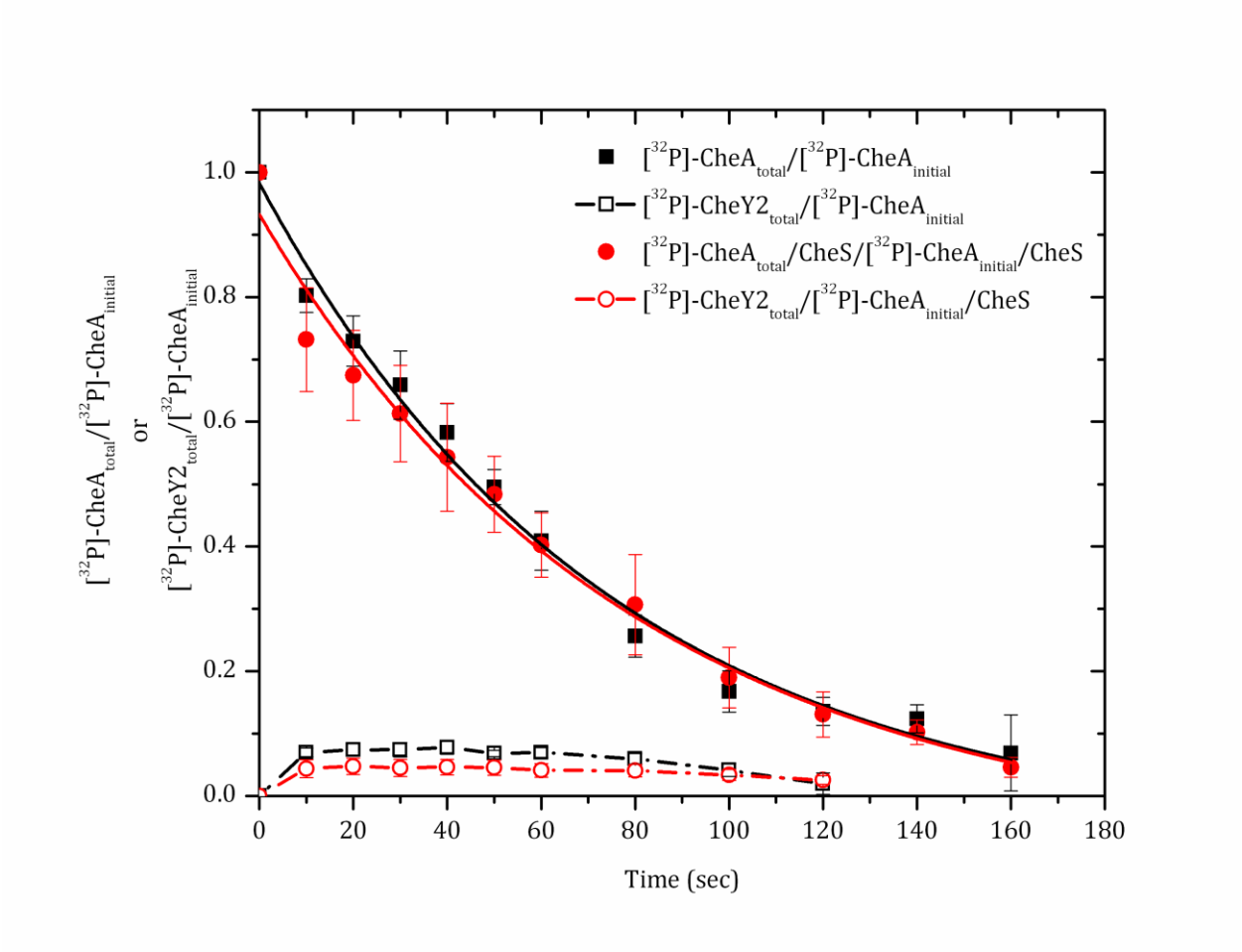

Figure 3.6. Time course of CheY2 dephosphorylation in the presence of CheA and CheA/CheS. All data points from three independent experiments, including [^{32}P]-CheA and [^{32}P]-CheY2 are normalized against the control sample of [^{32}P]-CheA taken before the addition of CheY2. [^{32}P]-CheA data points are represented as solid black squares and [^{32}P]-CheA/CheS data points as solid red circles. [^{32}P]-CheY2 data points in the presence of CheA are represented as open black squares and those in the presence of CheA/CheS are represented as open red circles. Black and red lines represent computer-generated least squares fits of the data to single exponential decay curves using Origin 8.1.

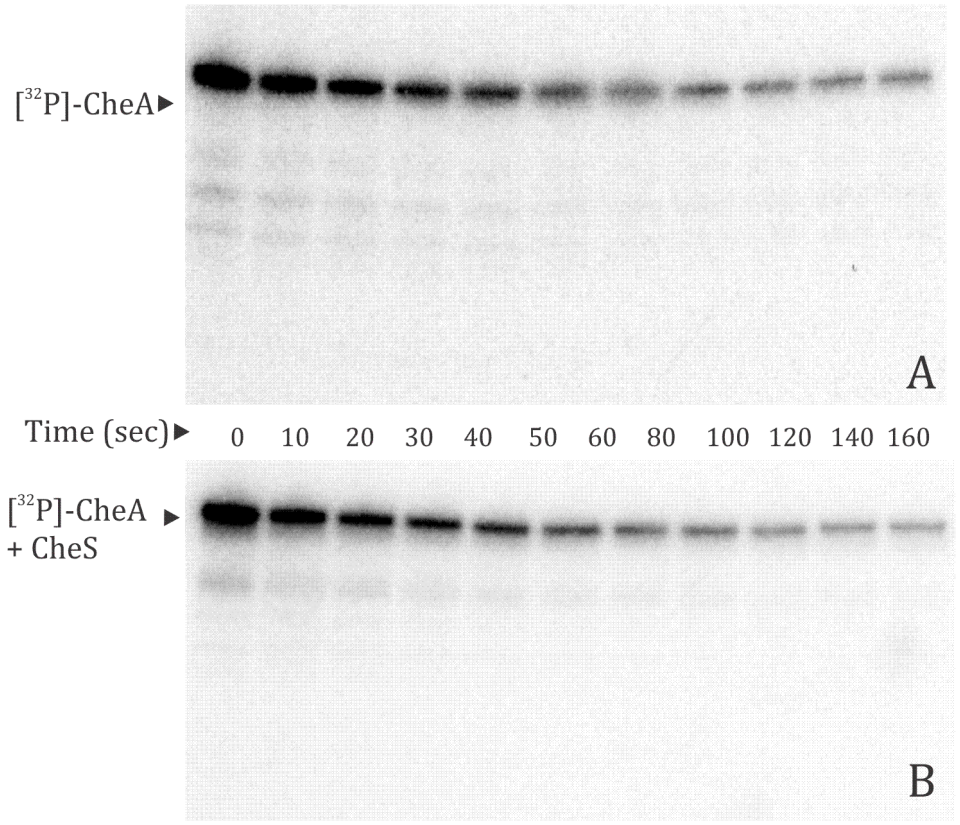

Figure 3.7. Autoradiogram indicating dephosphorylation of CheB following phosphotransfer from [^{32}P]phospho-CheA or CheA/CheS. A 10-fold molar excess of [^{32}P]-CheA or [^{32}P]-CheA/CheS was incubated with CheB at room temperature. Aliquots (20µl) were withdrawn at specified intervals, and the reaction was terminated by the addition of 10µl of 6X gel-loading buffer and 10mM EDTA. A 20µl aliquot of [^{32}P]-CheA or [^{32}P]-CheA/CheS was withdrawn before CheB addition and served as the control (C). After separation of the samples by SDS-PAGE, gels were exposed to a storage phosphor screen and the resultant image is shown above. (A) [^{32}P]-CheA and (B) [^{32}P]-CheA/CheS with CheB.

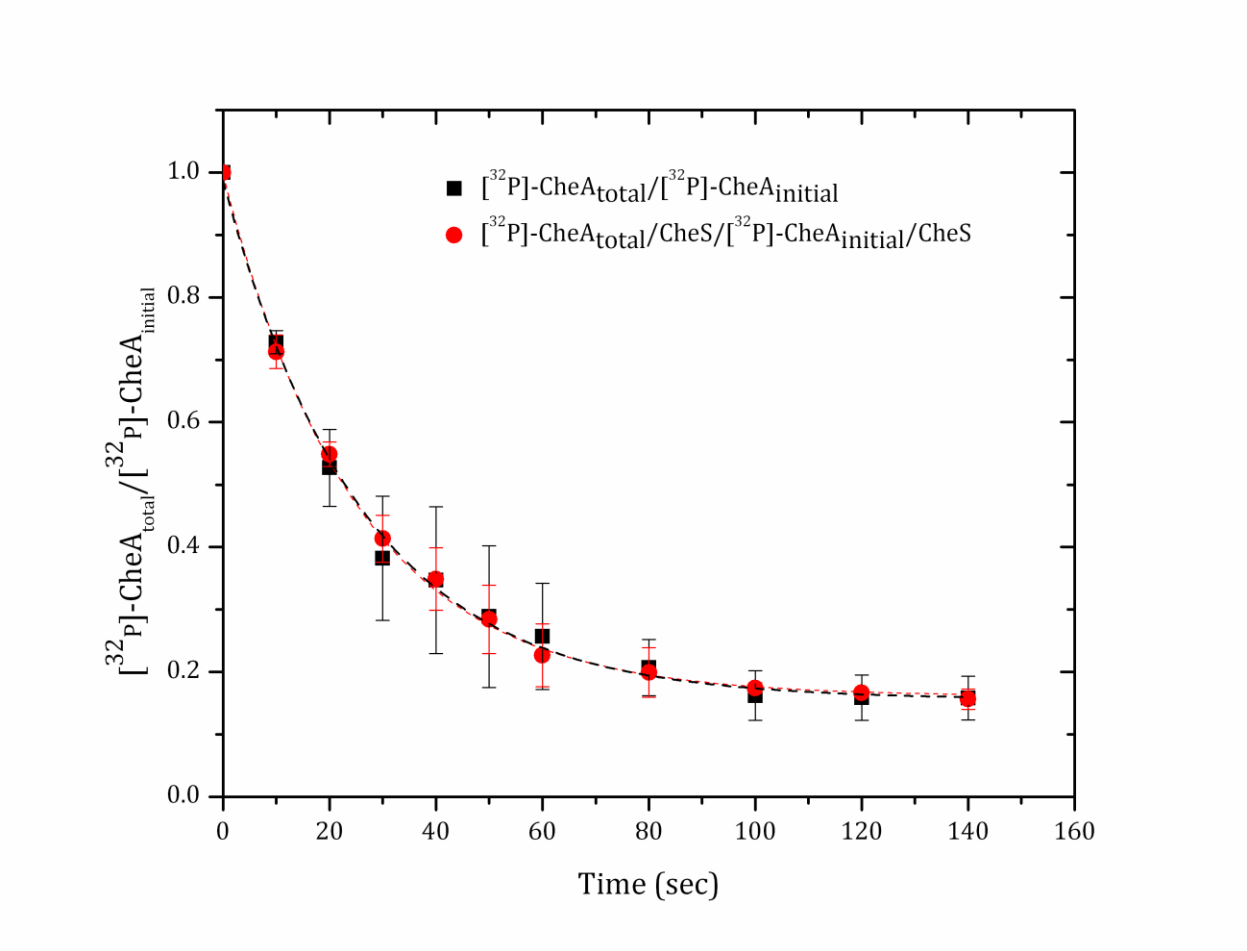

Figure 3.8. Time course of CheB dephosphorylation in the presence of CheA and CheA/CheS. All [^{32}P]-CheA data points from three independent experiments are normalized against the control sample of [^{32}P]-CheA taken before the addition of CheB. [^{32}P]-CheA data points are represented as solid black squares and [^{32}P]-CheA/CheS data points as solid red circles. Black and red lines represent computer-generated least squares fits of the data to single exponential decay curves using Origin 8.1.

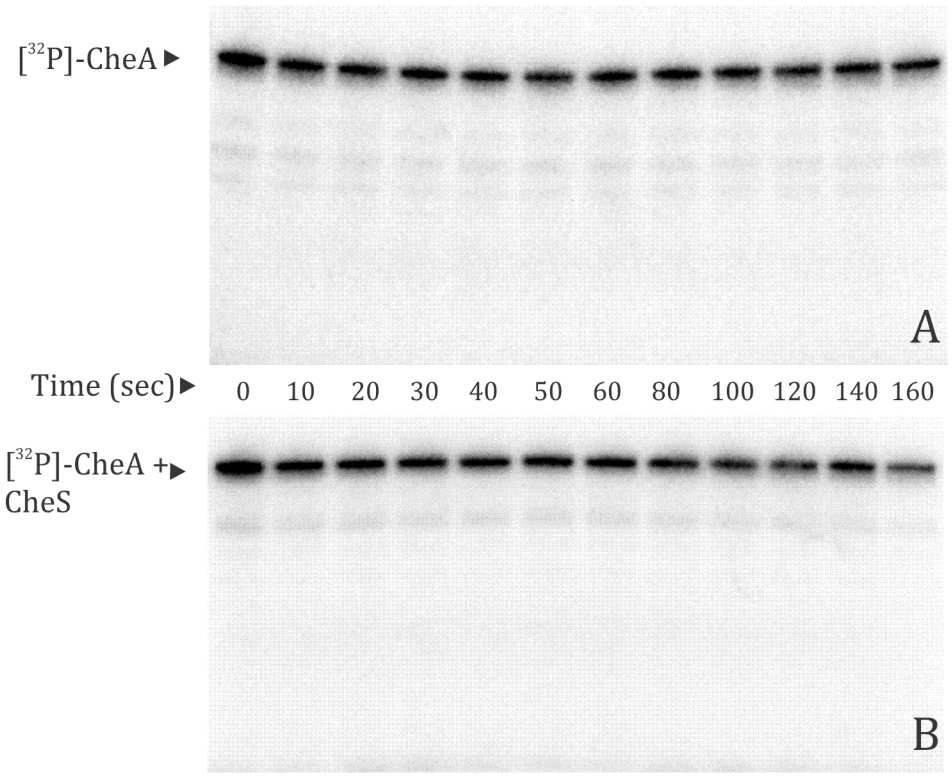

Figure 3.9. Autoradiogram showing autodephosphorylation of [^{32}P]phospho-CheA or CheA/CheS. 107pmoles of [^{32}P]-CheA or [^{32}P]-CheA/CheS were sampled at room temperature. Aliquots (20µl) were withdrawn at specified intervals, and the reaction was terminated by the addition of 10µl of 6X gel-loading buffer containing 10mM EDTA. A 20µl aliquot of [^{32}P]-CheA or [^{32}P]-CheA/CheS was withdrawn before TEDG addition and served as the control (C). After separation of the samples by SDS-PAGE, gels were exposed to a storage phosphor screen and the resultant image is shown above. (A) [^{32}P]-CheA and (B) [^{32}P]-CheA/CheS.

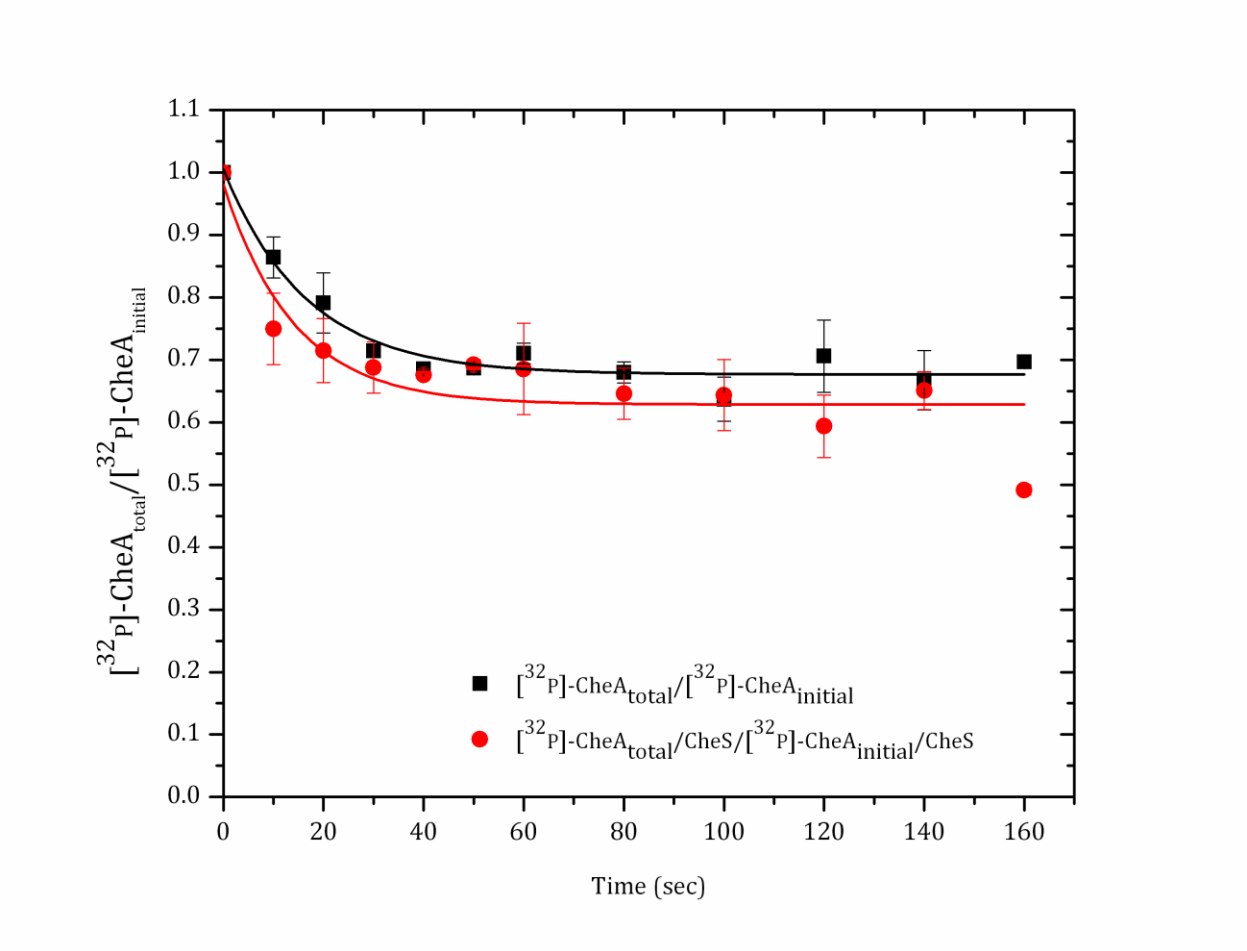

Figure 3.10. Time course of [^{32}P]phospho-CheA and CheA/CheS autodephosphorylation. All [^{32}P]-CheA data points from two independent experiments are normalized against the control sample of [^{32}P]-CheA taken before the addition of TEDG. [^{32}P]-CheA data points are represented as solid black squares and [^{32}P]-CheA/CheS data points as solid red circles. Black and red lines represent computer-generated least squares fits of the data to single exponential decay curves using Origin 8.1.

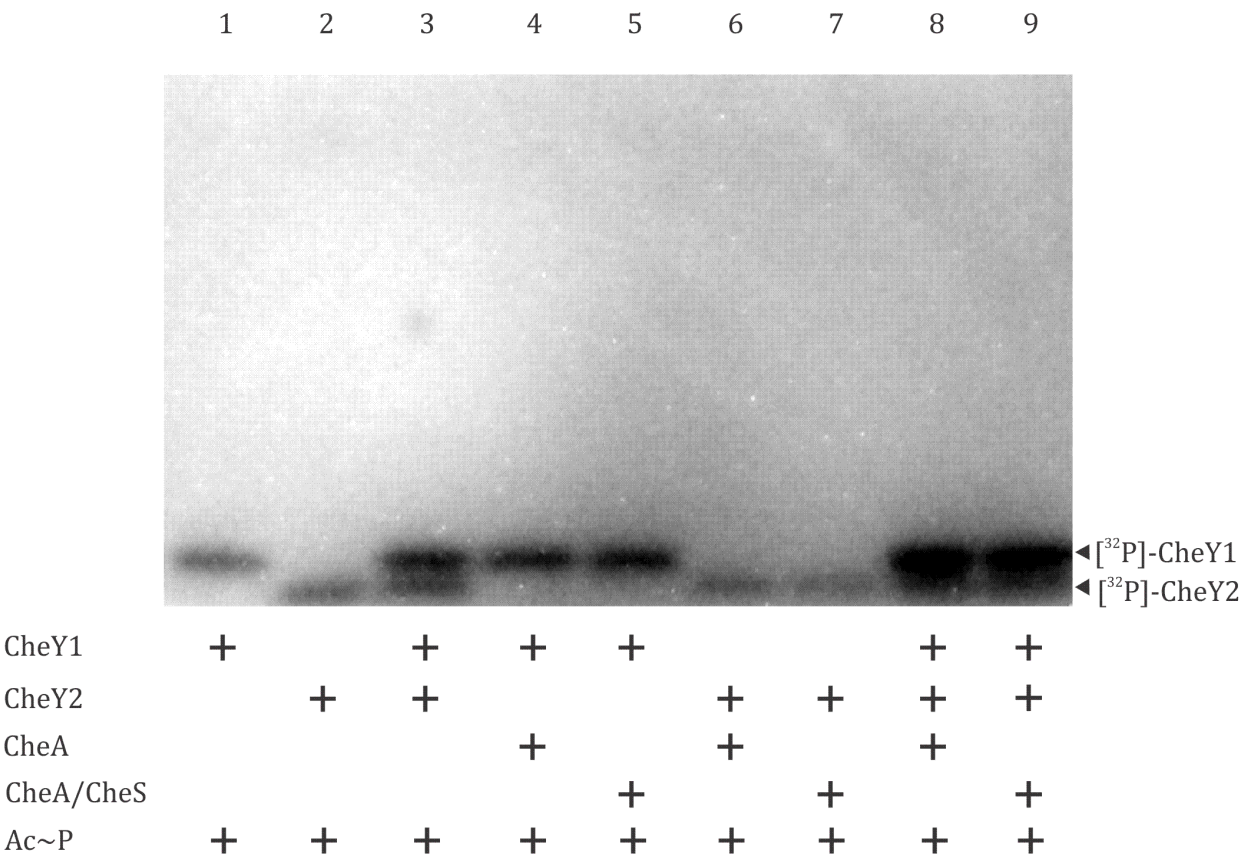

Figure 3.11. Autoradiogram showing phosphorylation of CheY1 and CheY2 with acetyl [^{32}P]phosphate. 20 µl reactions containing 5µM CheY1 and/or CheY2 were incubated with 18mM acetyl [^{32}P]phosphate in $TEDG_{10}$ containing 5mM $MgCl_2$ and 50mM KCl for 60s, after which $TEDG_{10}$, or 5µM CheA or CheA/CheS was added to the reaction and allowed to incubate for 20s. The reaction was stopped by the addition of 10µl of 6X gel-loading buffer containing 10mM EDTA. Samples were separated by electrophoresis and an autoradiogram was obtained.

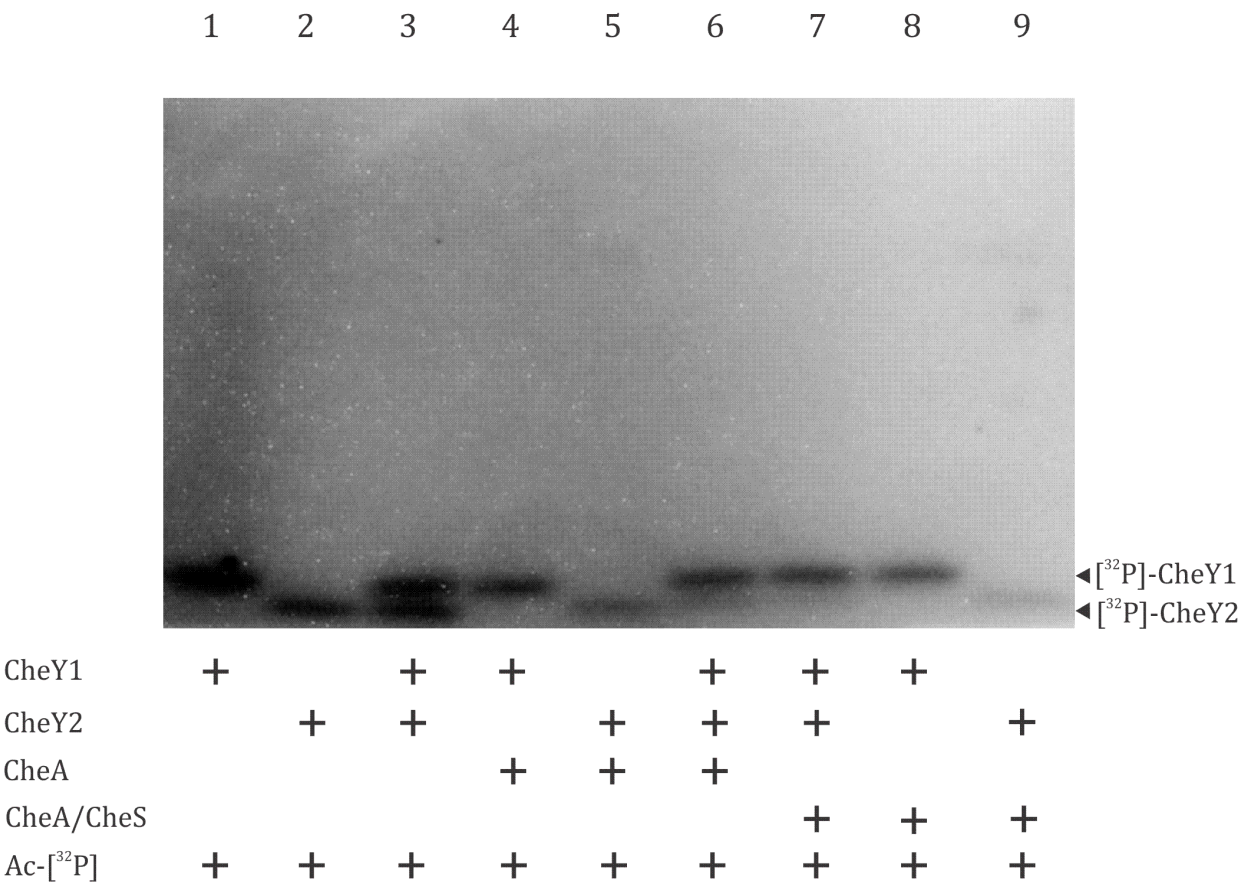

Figure 3.12. Second autoradiogram showing phosphorylation of CheY1 and CheY2 with acetyl [^{32}P]phosphate. 20 µl reactions containing 5µM CheY1 and/or CheY2 were incubated with 18mM acetyl [^{32}P]phosphate in $TEDG_{10}$ containing 5mM $MgCl_2$ and 50mM KCl for 60s, after which $TEDG_{10}$, or 5µM CheA or CheA/CheS was added to the reaction and allowed to incubate for 20s. The reaction was stopped by the addition of 10µl of 6X gel-loading buffer containing 10mM EDTA. Samples were separated by electrophoresis and an autoradiogram was obtained.

Chapter 4

Overall discussion

Dephosphorylation of the response regulator responsible for flagellar modulation by a specific phosphatase, most notably, CheZ in *E. coli*, is the traditional paradigm of signal termination in bacterial chemotaxis (12, 37, 65, 103). Alternative mechanisms for signal termination, such as the phosphate sink have been documented in various non-enteric bacteria lacking a CheZ homolog (5, 30, 60, 77, 94). In *S. meliloti*, a second response regulator, CheY1, serves as a phosphate sink, competing with CheY2 for phosphate from the active histidine kinase CheA~P (84). The phenotype of the *cheS* mutant of *S. meliloti* made us investigate other means of signal termination, which worked in parallel with the phosphate sink. In earlier experiments, the interaction of CheS with the autokinase CheA was established through *in vitro* and *in vivo* analyses (64, 100). Recombinant CheS was found to be obtained in a soluble and stable form in the presence of CheA or the P2 domain of CheA. These observations were confirmed by analyzing the expression of soluble CheS in the presence and absence of CheA by an immunoblot using polyclonal α-CheS antibodies. CheS was stable only in the presence of CheA. It is possible that CheS expressed in the absence of CheA, due to its hydrophobic nature, could have folded incorrectly, aggregated, and then been degraded by cytosolic proteases. The interaction of CheS exclusively with the P2 domain of CheA had been established by crosslinking experiments of refolded CheS (64). In co-expression and purification studies, the binding of CheS to the P2 domain of CheA was indicated by the stable expression of CheS with the $P2_{linker}$ domain (B. Scharf, personal communication). These observations were confirmed by probing CheS-CheA-domain complexes with α-CheS antibodies in immunoblots. CheS was found to be stably expressed only in the presence of the P2 domain, but not the P1 or P345 domains. The CheS binding domain on CheA was determined to be $CheA_{163-256}$, which overlapped the CheY2

binding domain, $CheA_{174-316}$. Thus, CheS was found to localize near the CheY2 binding domain on CheA.

Both CheY2 and CheY1 interact with CheA with varying affinities. CheY2 binds to the CheA with 500X higher affinity than CheY1 as determined by surface plasmon resonance (SPR) (66). Does CheS increase the binding affinity of CheY1 to CheA? If the binding affinity of CheY1 to CheA is increased, the rate of phosphotransfer between CheA~P and CheY1 might increase, accelerating the rate of signal termination. Phosphotransfer experiments indicated that CheS accelerates the rate of CheY1~P phosphorylation two-fold, but does not affect CheA autophosphorylation or the CheY2~P to CheA retrophosphorylation event. Based on the results from this work, a model for the role of CheS in signal termination can be envisioned.

Binding of CheS to the P2 domain of CheA may result in the change of the tertiary structure of CheA. The P2 domain of *S. meliloti* CheA shares very low sequence identity with the P2 domain of *E. coli* CheA (Appendix). While the P1, P34, and P5 domains of *S. meliloti* CheA share 35%, 47% and 38% identical residues with *E. coli* CheA, respectively, the P2 domains share only 18% identity. Additionally, the *S. meliloti* $P2_{linker}$ domain is 100 residues longer than that in *E. coli*, and contains 55 additional residues in the linker regions and 45 in the central domain (66). This might suggest a different or additional function of these residues in the P2 domain of *S. meliloti*. Four reactions in the phosphotransfer chain in *S. meliloti* chemotaxis were investigated to determine the role of CheS. The autophosphorylation of CheA is the first step in chemotaxis, but CheS did not play a role in this reaction. CheY1 and CheY2 are phosphorylated by CheA~P in the cell, and the resultant CheY1~P and CheY2~P

have a half-life of 12 sec and 10.5 sec, respectively (84). The possibility that CheY1~P or CheY2~P dephosphorylation may be accelerated by CheS was also investigated. Although CheS does not affect CheY2 dephosphorylation, it increases the dephosphorylation of CheY1 almost two-fold. Finally, an increase in the amount of retrophosphorylation from CheY2~P to CheA/CheS was not observed, either with or without CheY1 in the reaction. However, several factors could have influenced the outcome of the retrophosphorylation experiment. A two-fold increase in CheY1~P dephosphorylation due to the presence of CheS seems to be relatively small. However, one needs to take into account that these *in vitro* experiments did not include other components of the chemotaxis complex, such as CheW or chemoreceptors. If a soluble receptor such as IcpA in complex with CheW would be added to the *in vitro* system, the kinase or phosphotransferase state of the kinase can be more closely controlled.

A model for the role of CheS in signal termination

Given the acceleration of the dephosphorylation rate of CheY1~P by the presence of CheS bound to CheA, CheS may interact with CheY1 to either increase its affinity for the P2 domain of CheA, or change the tertiary structure of the CheY1 protein to cause it to dephosphorylate faster (Figure 4.1). CheS does not have a phosphatase motif, so it likely does not directly dephosphorylate CheY1. No evidence exists for an interaction between CheS and CheY1, as determined in earlier cross-linking experiments. However, it should be noted that in those experiments, refolded CheS was used which may not represent its native state (64). CheS can be co-purified with $CheA_{174\text{-}316}$. This complex presents CheS in a state relatively unencumbered by CheA. Repeating the cross-linking experiments with the $CheA_{174\text{-}316}$/CheS complex instead of refolded CheS might reveal its interaction with CheY1

and/or CheY2. Other experiments to establish CheS-CheY1 interaction include fluorescence resonance energy transfer (FRET) analysis, isothermal titration calorimetry (ITC) and the yeast-2-hybrid (Y2H) system. These analyses may add proof of the interaction between CheS and CheY1 *in vitro* and *in vivo*. Additionally, CheY1 could be phosphorylated by acetyl [^{32}P]phosphate and the rate of dephosphorylation of the active CheY1~P protein could be studied in a time course, with the decay of CheY1~P in the absence of the CheA/CheS complex acting as the control. In the proposed model, CheS, by virtue of its association with the P2 domain of CheA, may increase the affinity of P2 towards CheY1. This may result in a change of the tertiary structure of CheY1 resulting in faster dephosphorylation (Figure 4.1).

An alternative mode of action

It is possible that the activity of CheS is regulated by phosphorylation from a yet unknown kinase. Position-specific iterated-BLAST (PSI-BLAST) analysis of the CheS amino acid sequence indicated a homology (E value: 7.07e-04) of CheS with the Sulfate transporter anti-sigma factor antagonist (STAS) domain, found in anti-anti-sigma factors such as SpoIIAA in *B. subtilis* (4). SpoIIAA is phosphorylated by the kinase SpoIIAB at a conserved Ser residue, resulting in its activation (44). Interestingly, the CheS sequence contains a conserved Ser residue at position 75. This residue could be phosphorylated by a yet unknown kinase resulting in phospho-CheS. To test the possibility of this residue being phosphorylated *in vivo*, the conserved Ser could be replaced with another residue such as Ala. The resulting phenotype would reveal the importance of this residue in signal termination and indicate its function in CheS activation in the cell. In its active state, CheS could directly interact with CheY1 and/or CheY2. It could then either affect the activation state of CheA or result in the faster dephosphosphorylation of CheY1~P (Figure 4.2). To

determine the kinase responsible for CheS phosphorylation, a genome wide search for yet uncharacterized genes encoding serine kinases in *S. meliloti* could be performed.

At the current time, it is certain that CheS interacts with the P2 domain of CheA. While further research is needed to display the possible interaction of CheS with CheY1, the interaction of CheS with the P2 domain should be studied in detail. Such studies would reveal the three dimensional structure of CheS and provide insight into the interaction of CheS and the P2 domain and the intermolecular bonds responsible for this association. An effort was made to co-crystallize the $CheA_{174-316}$/CheS complex in collaboration with Dr. Ann Stock's laboratory at Rutgers University. The $CheA_{174-316}$ sequence is essentially the binding sequence of CheY2 on CheA (66). Despite various efforts to co-crystallize the complex, no crystals were obtained. Future work would be necessary to try and obtain the X-ray crystal structure of CheS with the P2 domain.

Final Remarks

Bacterial motility is an important aspect of host-microbe interactions, whether these interactions are parasitic or symbiotic. *S. meliloti* utilizes chemotaxis to sense and respond to the soil environment, and to form interactions with its plant hosts. Ease of manipulation of the *S. meliloti* genome, and its published whole genome sequence makes it a model organism to study host-microbe interactions, including chemotaxis (20). The arrangement of the *che1* operon in *S. meliloti* is shared by other members of the α-proteobacteria such as *Agrobacterium¸ Caulobacter* and *Rhodobacter.* The genome of these organisms contains a gene of unknown function at the second position in their chemotaxis operons. These genes encode proteins that share sequence homology with CheS. Understanding the role of CheS would provide greater insight into signal termination in chemotaxis in *S. meliloti*, and by extension, in other members of the α-proteobacteria. Further analysis of CheS interaction with the P2 domain of CheA, and with response regulators such as CheY1 and CheY2 is required to fully delineate its role in the chemotaxis phosphate flux. My work has contributed to a clearer understanding of CheS binding to the CheA-P2 domain, and has provided evidence for an acceleration of CheY1 dephosphorylation in the presence of CheS. This opens up exciting avenues of further research which would reveal interactions and pathways that would add substantially to the knowledge of chemotaxis in general, and signal termination through a phosphate sink in particular.

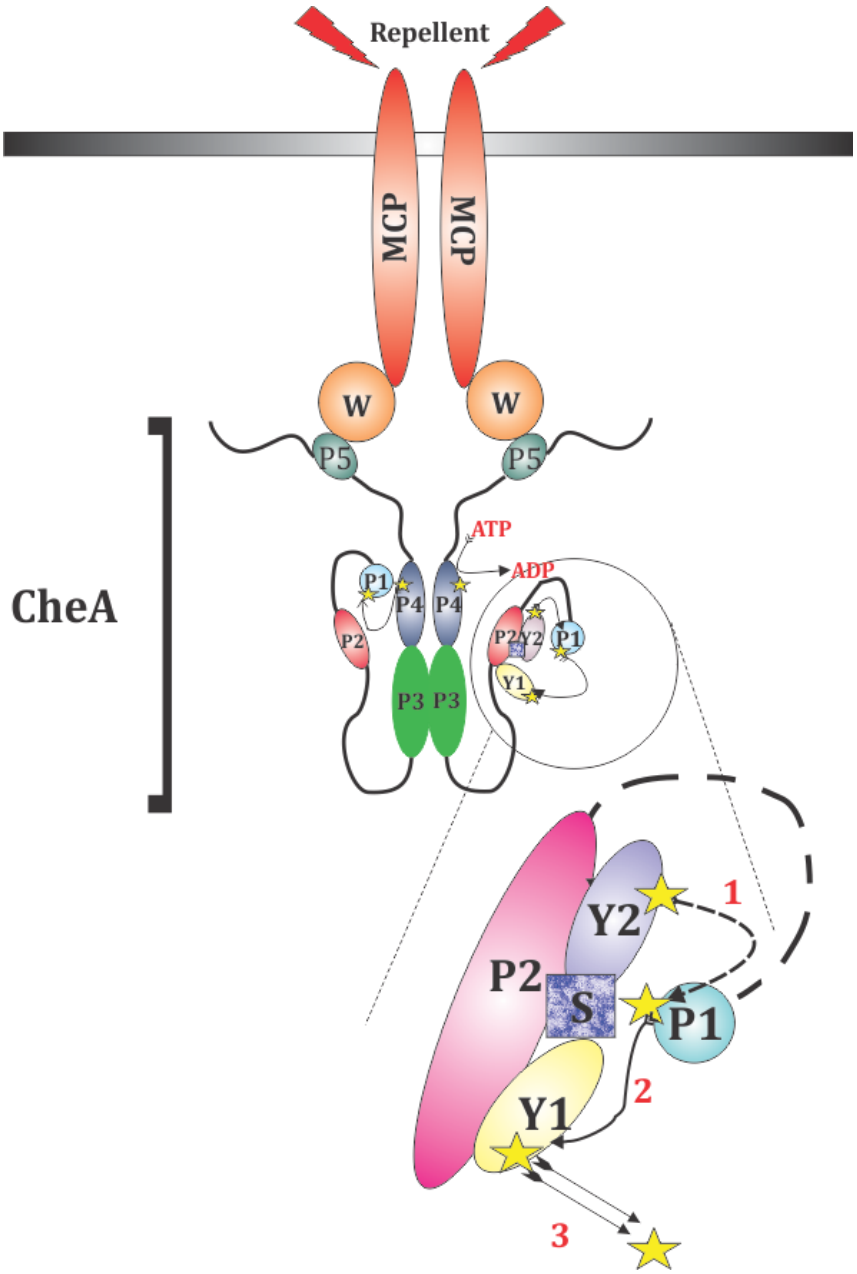

Figure 4.1. Proposed model for signal termination in the *S. meliloti* chemotaxis pathway where CheS binds to CheA and accelerates the dephosphorylation of CheY1~P. Here, CheY2~P retro-transfers the phosphate to CheY1 through CheA. CheS binds to the P2 domain and increases the binding affinity of CheY1 to P2. CheY2~P transfers its phosphate group to the P1 domain (Step 1). P1 can then transfer the phosphate to CheY1 (Step 2). CheY1 dephosphorylates at a higher rate due to its interaction with CheS (Step 3). Dephosphorylation of CheY1 shifts the equilibrium towards CheY1 and the rate of signal termination is accelerated.

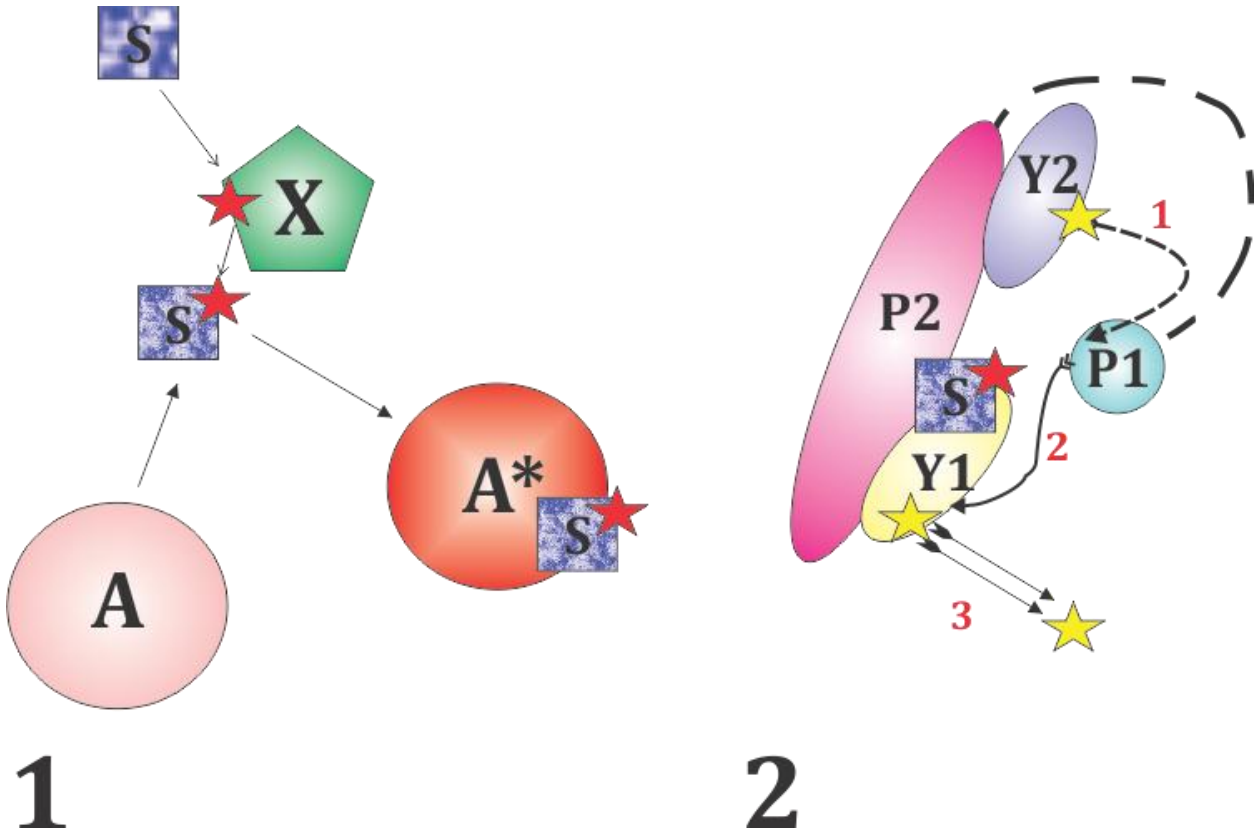

Figure 4.2. Alternate models for signal termination in which CheS may be phosphorylated at Ser-75 by a yet unknown kinase (X). In the first scenario, activated CheS could interact with CheA, switching it to a phosphotransferase ON state, in which CheA favors retrophosphorylation. Or, in the second scenario, activated CheS may directly interact with CheY1 accelerating the dephosphorylation of CheY1~P (Step 3).

REFERENCES

1. **Adler, J.** 1966. Effect of amino acids and oxygen on chemotaxis in *Escherichia coli*. J Bacteriol **92:**121-129.

2. **Altschul, S. F., T. L. Madden, A. A. Schaffer, J. Zhang, Z. Zhang, W. Miller, and D. J. Lipman.** 1997. Gapped BLAST and PSI-BLAST: a new generation of protein database search programs. Nucleic Acids Res **25:**3389-3402.

3. **Antommattei, F. M., J. B. Munzner, and R. M. Weis.** 2004. Ligand-specific activation of *Escherichia coli* chemoreceptor transmethylation. J Bacteriol **186:**7556-7563.

4. **Aravind, L., and E. V. Koonin.** 2000. The STAS domain - a link between anion transporters and antisigma-factor antagonists. Curr Biol **10:**R53-55.

5. **Armitage, J. P., and R. Schmitt.** 1997. Bacterial chemotaxis: *Rhodobacter sphaeroides* and *Sinorhizobium meliloti*--variations on a theme? Microbiology **143 (Pt 12):**3671-3682.

6. **Armitage, J. P., Schmitt, R.** 1997. Bacterial chemotaxis: *Rhodobacter sphaeroides* and *Sinorhizobium meliloti* - variations on a theme? Microbiology **143:**3671-3682.

7. **Babic, K. H., K. Schauss, B. Hai, S. Sikora, S. Redzepovic, V. Radl, and M. Schloter.** 2008. Influence of different *Sinorhizobium meliloti* inocula on abundance of genes involved in nitrogen transformations in the rhizosphere of alfalfa (*Medicago sativa* L.). Environmental microbiology **10:**2922-2930.

8. **Bachmann, B. J.** 1990. Linkage map of *Escherichia coli* K-12, edition 8. Microbiol Rev **54:**130-197.

9. **Berg, H. C., and D. A. Brown.** 1974. Chemotaxis in *Escherichia coli* analyzed by three-dimensional tracking. Antibiot Chemother **19:**55-78.

10. **Berg, H. C., and E. M. Purcell.** 1977. Physics of chemoreception. Biophys J **20:**193-219.

11. **Bilwes, A. M., L. A. Alex, B. R. Crane, and M. I. Simon.** 1999. Structure of CheA, a signal-transducing histidine kinase. Cell **96:**131-141.

12. **Blat, Y., and M. Eisenbach.** 1994. Phosphorylation-dependent binding of the chemotaxis signal molecule CheY to its phosphatase, CheZ. Biochemistry **33:**902-906.

13. **Boukhvalova, M. S., F. W. Dahlquist, and R. C. Stewart.** 2002. CheW binding interactions with CheA and Tar. Importance for chemotaxis signaling in *Escherichia coli*. J Biol Chem **277:**22251-22259.

14. **Bourret, R. B., J. F. Hess, and M. I. Simon.** 1990. Conserved aspartate residues and phosphorylation in signal transduction by the chemotaxis protein CheY. Proc Natl Acad Sci U S A **87:**41-45.

15. **Brown, D. A., and H. C. Berg.** 1974. Temporal stimulation of chemotaxis in *Escherichia coli.* Proc Natl Acad Sci U S A **71:**1388-1392.

16. **Eggenhofer, E., M. Haslbeck, and B. Scharf.** 2004. MotE serves as a new chaperone specific for the periplasmic motility protein, MotC, in *Sinorhizobium meliloti*. Mol Microbiol **52:**701-712.

17. **Ehrenberg, C. G.** 1838. Die Infusionsthierchen als vollkommene Organismen: ein Blick in das tiefere organische Leben der Natur, Nebst Einem Atlas von vierundsechzig colorierten Kupfertafeln (The infusoria as complete organisms: a look deeper into the organic life of nature, together with a colorized Atlas of sixty-four copper plates). *In* S. P. K. Akademie der Wissenschaften zu St. Petersburg (Royal Academy of Sciences (ed.). Leopold Voss, Leipzig.

18. **Eisenbach, M.** 1990. Functions of the flagellar modes of rotation in bacterial motility and chemotaxis. Mol Microbiol **4:**161-167.

19. **Eisenbach, M., A. Wolf, M. Welch, S. R. Caplan, I. R. Lapidus, R. M. Macnab, H. Aloni, and O. Asher.** 1990. Pausing, switching and speed fluctuation of the bacterial flagellar motor and their relation to motility and chemotaxis. J Mol Biol **211:**551-563.

20. **Galibert, F., T. M. Finan, S. R. Long, A. Puhler, P. Abola, F. Ampe, F. Barloy-Hubler, M. J. Barnett, A. Becker, P. Boistard, G. Bothe, M. Boutry, L. Bowser, J. Buhrmester, E. Cadieu, D. Capela, P. Chain, A. Cowie, R. W. Davis, S. Dreano, N. A. Federspiel, R. F. Fisher, S. Gloux, T. Godrie, A. Goffeau, B. Golding, J. Gouzy, M. Gurjal, I. Hernandez-Lucas, A. Hong, L. Huizar, R. W. Hyman, T. Jones, D. Kahn, M. L. Kahn, S. Kalman, D. H. Keating, E. Kiss, C. Komp, V. Lelaure, D. Masuy, C. Palm, M. C. Peck, T. M. Pohl, D. Portetelle, B. Purnelle, U. Ramsperger, R. Surzycki, P. Thebault, M. Vandenbol, F. J. Vorholter, S. Weidner, D. H. Wells, K. Wong, K. C. Yeh, and J. Batut.** 2001. The composite genome of the legume symbiont *Sinorhizobium meliloti.* Science **293:**668-672.

21. **Garzon, A., and J. S. Parkinson.** 1996. Chemotactic signaling by the P1 phosphorylation domain liberated from the CheA histidine kinase of *Escherichia coli*. J Bacteriol **178:**6752-6758.

22. **Goetz, R., and R. Schmitt.** 1987. *Rhizobium meliloti* swims by unidirectional, intermittent rotation of right-handed flagellar helices. J Bacteriol **169:**3146-3150.

23. **Greck, M., J. Platzer, V. Sourjik, and R. Schmitt.** 1995. Analysis of a chemotaxis operon in *Rhizobium meliloti*. Mol Microbiol **15:**989-1000.

24. **Gurich, N., and J. E. Gonzalez.** 2009. Role of quorum sensing in *Sinorhizobium meliloti*-Alfalfa symbiosis. J Bacteriol **191:**4372-4382.

25. **Hamel, D. J., H. Zhou, M. R. Starich, R. A. Byrd, and F. W. Dahlquist.** 2006. Chemical-shift-perturbation mapping of the phosphotransfer and catalytic domain interaction in the histidine autokinase CheA from *Thermotoga maritima*. Biochemistry **45:**9509-9517.

26. **Hanahan, D., and M. Meselson.** 1983. Plasmid screening at high colony density. Methods Enzymol **100:**333-342.

27. **Hess, J. F., K. Oosawa, N. Kaplan, and M. I. Simon.** 1988. Phosphorylation of three proteins in the signaling pathway of bacterial chemotaxis. Cell **53:**79-87.

28. **Hess, J. F., K. Oosawa, P. Matsumura, and M. I. Simon.** 1987. Protein phosphorylation is involved in bacterial chemotaxis. Proc Natl Acad Sci U S A **84:**7609-7613.

29. **Jahreis, K., T. B. Morrison, A. Garzon, and J. S. Parkinson.** 2004. Chemotactic signaling by an *Escherichia coli* CheA mutant that lacks the binding domain for phosphoacceptor partners. J Bacteriol **186:**2664-2672.

30. **Jimenez-Pearson, M. A., I. Delany, V. Scarlato, and D. Beier.** 2005. Phosphate flow in the chemotactic response system of *Helicobacter pylori*. Microbiology **151:**3299-3311.

31. **Jones, K. M., H. Kobayashi, B. W. Davies, M. E. Taga, and G. C. Walker.** 2007. How rhizobial symbionts invade plants: the *Sinorhizobium*-Medicago model. Nat Rev Micro **5:**619-633.

32. **Kamiya, R., H. Hotani, and S. Asakura.** 1982. Polymorphic transition in bacterial flagella. Symp Soc Exp Biol **35:**53-76.

33. **Kehry, M. R., and F. W. Dahlquist.** 1982. Adaptation in bacterial chemotaxis: CheB-dependent modification permits additional methylations of sensory transducer proteins. Cell **29:**761-772.

34. **Kleene, S. J., A. C. Hobson, and J. Adler.** 1979. Attractants and repellents influence methylation and demethylation of methyl-accepting chemotaxis proteins in an extract of *Escherichia coli*. Proc Natl Acad Sci U S A **76:**6309-6313.

35. **Kleene, S. J., M. L. Toews, and J. Adler.** 1977. Isolation of glutamic acid methyl ester from an *Escherichia coli* membrane protein involved in chemotaxis. J Biol Chem **252:**3214-3218.

36. **Krupski, G., R. Gotz, K. Ober, E. Pleier, and R. Schmitt.** 1985. Structure of complex flagellar filaments in *Rhizobium meliloti*. J Bacteriol **162:**361-366.

37. **Kuo, S. C., and D. E. Koshland, Jr.** 1987. Roles of cheY and cheZ gene products in controlling flagellar rotation in bacterial chemotaxis of *Escherichia coli*. J Bacteriol **169:**1307-1314.

38. **Li, M., and G. L. Hazelbauer.** 2004. Cellular stoichiometry of the components of the chemotaxis signaling complex. J Bacteriol **186:**3687-3694.

39. **Lipmann F., T. L. C.** 1945. A specific micromethod for the detection of acyl phosphates. J. Biol. Chem. **159:**21-28.

40. **Lloyd, S. A., H. Tang, X. Wang, S. Billings, and D. F. Blair.** 1996. Torque generation in the flagellar motor of *Escherichia coli*: evidence of a direct role for FliG but not for FliM or FliN. J Bacteriol **178:**223-231.

41. **Lupas, A., and J. Stock.** 1989. Phosphorylation of an N-terminal regulatory domain activates the CheB methylesterase in bacterial chemotaxis. J Biol Chem **264:**17337-17342.

42. **Macnab, R. M., and D. E. Koshland, Jr.** 1972. The gradient-sensing mechanism in bacterial chemotaxis. Proc Natl Acad Sci U S A **69:**2509-2512.

43. **Macnab, R. M., and M. K. Ornston.** 1977. Normal-to-curly flagellar transitions and their role in bacterial tumbling. Stabilization of an alternative quaternary structure by mechanical force. J Mol Biol **112:**1-30.

44. **Masuda, S., K. S. Murakami, S. Wang, C. Anders Olson, J. Donigian, F. Leon, S. A. Darst, and E. A. Campbell.** 2004. Crystal structures of the ADP and ATP bound forms of the *Bacillus* anti-sigma factor SpoIIAB in complex with the anti-anti-sigma SpoIIAA. J Mol Biol **340:**941-956.

45. **Matagne, A., B. Joris, and J. M. Frere.** 1991. Anomalous behaviour of a protein during SDS/PAGE corrected by chemical modification of carboxylic groups. Biochem J **280 (Pt 2):**553-556.

46. **McCleary, W. R., and J. B. Stock.** 1994. Acetyl phosphate and the activation of two-component response regulators. J Biol Chem **269:**31567-31572.

47. **McGuffin, L. J., K. Bryson, and D. T. Jones.** 2000. The PSIPRED protein structure prediction server. Bioinformatics **16:**404-405.

48. **Meier, V. M., and B. E. Scharf.** 2009. Cellular localization of predicted transmembrane and soluble chemoreceptors in *Sinorhizobium meliloti*. J Bacteriol **191:**5724-5733.

49. **Mesibov, R., and J. Adler.** 1972. Chemotaxis toward amino acids in *Escherichia coli*. J Bacteriol **112:**315-326.

50. **Min, K. T., C. M. Hilditch, B. Diederich, J. Errington, and M. D. Yudkin.** 1993. Sigma F, the first compartment-specific transcription factor of *B. subtilis*, is regulated by an anti-sigma factor that is also a protein kinase. Cell **74:**735-742.

51. **Morgan, D. G., R. M. Macnab, N. R. Francis, and D. J. DeRosier.** 1993. Domain organization of the subunit of the *Salmonella typhimurium* flagellar hook. J Mol Biol **229:**79-84.

52. **Novick, R. P., R. C. Clowes, S. N. Cohen, R. Curtiss, 3rd, N. Datta, and S. Falkow.** 1976. Uniform nomenclature for bacterial plasmids: a proposal. Bacteriol Rev **40:**168-189.

53. **Olivera, B. C., E. Ugalde, and A. Martinez-Antonio.** 2010. Regulatory dynamics of standard two-component systems in bacteria. J Theor Biol **264:**560-569.

54. **Ottemann, K. M., W. Xiao, Y. K. Shin, and D. E. Koshland, Jr.** 1999. A piston model for transmembrane signaling of the aspartate receptor. Science **285:**1751-1754.

55. **Park, S. Y., X. Chao, G. Gonzalez-Bonet, B. D. Beel, A. M. Bilwes, and B. R. Crane.** 2004. Structure and function of an unusual family of protein phosphatases: the bacterial chemotaxis proteins CheC and CheX. Mol Cell **16:**563-574.

56. **Peck, M. C., R. F. Fisher, and S. R. Long.** 2006. Diverse flavonoids stimulate NodD1 binding to nod gene promoters in *Sinorhizobium meliloti*. J Bacteriol **188:**5417-5427.

57. **Perego, M., C. Hanstein, K. M. Welsh, T. Djavakhishvili, P. Glaser, and J. A. Hoch.** 1994. Multiple protein-aspartate phosphatases provide a mechanism for the integration of diverse signals in the control of development in *B. subtilis*. Cell **79:**1047-1055.

58. **Perret, X., C. Staehelin, and W. J. Broughton.** 2000. Molecular basis of symbiotic promiscuity. Microbiol Mol Biol Rev **64:**180-201.

59. **Pfeffer, W.** 1883. Locomotorische richtungsbewegungen durch chemische reize (Locomotory direction movements by chemical stimuli). Berichte deutsch bot ges **1:**524-533.

60. **Pittman, M. S., M. Goodwin, and D. J. Kelly.** 2001. Chemotaxis in the human gastric pathogen *Helicobacter pylori*: different roles for CheW and the three CheV paralogues, and evidence for CheV2 phosphorylation. Microbiology **147:**2493-2504.

61. **Platzer, J., W. Sterr, M. Hausmann, and R. Schmitt.** 1997. Three genes of a motility operon and their role in flagellar rotary speed variation in *Rhizobium meliloti*. J Bacteriol **179:**6391-6399.

62. **Pleier, E., and R. Schmitt.** 1991. Expression of two *Rhizobium meliloti* flagellin genes and their contribution to the complex filament structure. J Bacteriol **173:**2077-2085.

63. **Pottathil, M., and B. A. Lazazzera.** 2003. The extracellular Phr peptide-Rap phosphatase signaling circuit of *Bacillus subtilis*. Frontiers in bioscience : a journal and virtual library **8:**d32-45.

64. **Purschke, F.** 2007. Untersuchungen zur Funktion von CheX in der chemotaktischen Signalkette von *Sinorhizobium meliloti* (Studies on the function of Chex in the chemotactic signaling pathway of *Sinorhizobium meliloti*). Universität Regensburg, Regensburg.

65. **Rao, C. V., J. R. Kirby, and A. P. Arkin.** 2005. Phosphatase localization in bacterial chemotaxis: divergent mechanisms, convergent principles. Phys Biol **2:**148-158.

66. **Riepl, H., T. Maurer, H. R. Kalbitzer, V. M. Meier, M. Haslbeck, R. Schmitt, and B. Scharf.** 2008. Interaction of CheY2 and CheY2-P with the cognate CheA kinase in the chemosensory-signalling chain of *Sinorhizobium meliloti*. Mol Microbiol **69:**1373-1384.

67. **Rosario, M. M., and G. W. Ordal.** 1996. CheC and CheD interact to regulate methylation of *Bacillus subtilis* methyl-accepting chemotaxis proteins. Mol Microbiol **21:**511-518.

68. **Rowsell, E. H., J. M. Smith, A. Wolfe, and B. L. Taylor.** 1995. CheA, CheW, and CheY are required for chemotaxis to oxygen and sugars of the phosphotransferase system in *Escherichia coli*. J Bacteriol **177:**6011-6014.

69. **Samatey, F. A., K. Imada, S. Nagashima, F. Vonderviszt, T. Kumasaka, M. Yamamoto, and K. Namba.** 2001. Structure of the bacterial flagellar protofilament and implications for a switch for supercoiling. Nature **410:**331-337.

70. **Samatey, F. A., H. Matsunami, K. Imada, S. Nagashima, T. R. Shaikh, D. R. Thomas, J. Z. Chen, D. J. Derosier, A. Kitao, and K. Namba.** 2004. Structure of the bacterial flagellar hook and implication for the molecular universal joint mechanism. Nature **431:**1062-1068.

71. **Scharf, B., and R. Schmitt.** 2002. Sensory transduction to the flagellar motor of *Sinorhizobium meliloti*. J Mol Microbiol Biotechnol **4:**183-186.

72. **Scharf, B., H. Schuster-Wolff-Buhring, R. Rachel, and R. Schmitt.** 2001. Mutational analysis of the *Rhizobium lupini* H13-3 and *Sinorhizobium meliloti* flagellin genes: importance of flagellin A for flagellar filament structure and transcriptional regulation. J Bacteriol **183:**5334-5342.

73. **Scharf, B. E., K. A. Fahrner, L. Turner, and H. C. Berg.** 1998. Control of direction of flagellar rotation in bacterial chemotaxis. Proc Natl Acad Sci U S A **95:**201-206.

74. **Schmitt, R.** 2002. Sinorhizobial chemotaxis: a departure from the enterobacterial paradigm. Microbiology **148:**627-631.

75. **Schmitt, R., I. Raska, and F. Mayer.** 1974. Plain and complex flagella of *Pseudomonas rhodos*: analysis of fine structure and composition. J Bacteriol **117:**844-857.

76. **Segall, J. E., S. M. Block, and H. C. Berg.** 1986. Temporal comparisons in bacterial chemotaxis. Proc Natl Acad Sci U S A **83:**8987-8991.

77. **Shah, D. S., S. L. Porter, A. C. Martin, P. A. Hamblin, and J. P. Armitage.** 2000. Fine tuning bacterial chemotaxis: analysis of *Rhodobacter sphaeroides* behaviour under aerobic and anaerobic conditions by mutation of the major chemotaxis operons and cheY genes. EMBO J **19:**4601-4613.

78. **Silverman, M., P. Matsumura, M. Hilmen, and M. Simon.** 1977. Characterization of lambda *Escherichia coli* hybrids carrying chemotaxis genes. J Bacteriol **130:**877-887.

79. **Silverman, M., and M. Simon.** 1977. Identification of polypeptides necessary for chemotaxis in *Escherichia coli*. J Bacteriol **130:**1317-1325.

80. **Silversmith, R. E., G. P. Guanga, L. Betts, C. Chu, R. Zhao, and R. B. Bourret.** 2003. CheZ-mediated dephosphorylation of the *Escherichia coli* chemotaxis response regulator CheY: role for CheY glutamate 89. J Bacteriol **185:**1495-1502.

81. **Silversmith, R. E., M. D. Levin, E. Schilling, and R. B. Bourret.** 2008. Kinetic characterization of catalysis by the chemotaxis phosphatase CheZ. Modulation of activity by the phosphorylated CheY substrate. J Biol Chem **283:**756-765.

82. **Simon, R., M. O'Connell, M. Labes, and A. Puhler.** 1986. Plasmid vectors for the genetic analysis and manipulation of rhizobia and other gram-negative bacteria. Methods Enzymol **118:**640-659.

83. **Sourjik, V., and R. Schmitt.** 1996. Different roles of CheY1 and CheY2 in the chemotaxis of *Rhizobium meliloti*. Mol Microbiol **22:**427-436.

84. **Sourjik, V., and R. Schmitt.** 1998. Phosphotransfer between CheA, CheY1, and CheY2 in the chemotaxis signal transduction chain of *Rhizobium meliloti*. Biochemistry **37:**2327-2335.

85. **Sowa, Y., A. D. Rowe, M. C. Leake, T. Yakushi, M. Homma, A. Ishijima, and R. M. Berry.** 2005. Direct observation of steps in rotation of the bacterial flagellar motor. Nature **437:**916-919.

86. **Stadtman, E. R.** 1957. Preparation and assay of acetyl phosphate, p. 228-231, Methods in Enzymology, vol. Volume 3. Academic Press.

87. **Stewart, R. C., C. B. Russell, A. F. Roth, and F. W. Dahlquist.** 1988. Interaction of CheB with chemotaxis signal transduction components in *Escherichia coli*: modulation of the methylesterase activity and effects on cell swimming behavior. Cold Spring Harb Symp Quant Biol **53 Pt 1:**27-40.

88. **Stewart, R. C., and R. Van Bruggen.** 2004. Association and dissociation kinetics for CheY interacting with the P2 domain of CheA. J Mol Biol **336:**287-301.

89. **Stock, A. M., and J. B. Stock.** 1987. Purification and characterization of the CheZ protein of bacterial chemotaxis. J Bacteriol **169:**3301-3311.

90. **Surette, M. G., M. Levit, Y. Liu, G. Lukat, E. G. Ninfa, A. Ninfa, and J. B. Stock.** 1996. Dimerization is required for the activity of the protein histidine kinase CheA that mediates signal transduction in bacterial chemotaxis. J Biol Chem **271:**939-945.

91. **Swanson, R. V., S. C. Schuster, and M. I. Simon.** 1993. Expression of CheA fragments which define domains encoding kinase, phosphotransfer, and CheY binding activities. Biochemistry **32:**7623-7629.

92. **Szurmant, H., M. W. Bunn, V. J. Cannistraro, and G. W. Ordal.** 2003. *Bacillus subtilis* hydrolyzes CheY-P at the location of its action, the flagellar switch. J Biol Chem **278:**48611-48616.

93. **Szurmant, H., T. J. Muff, and G. W. Ordal.** 2004. *Bacillus subtilis* CheC and FliY are members of a novel class of CheY-P-hydrolyzing proteins in the chemotactic signal transduction cascade. J Biol Chem **279:**21787-21792.

94. **Szurmant, H., and G. W. Ordal.** 2004. Diversity in chemotaxis mechanisms among the bacteria and archaea. Microbiol Mol Biol Rev **68:**301-319.

95. **Tawa, P., and R. C. Stewart.** 1994. Kinetics of CheA autophosphorylation and dephosphorylation reactions. Biochemistry **33:**7917-7924.

96. **Thompson, J. D., T. J. Gibson, and D. G. Higgins.** 2002. Multiple sequence alignment using ClustalW and ClustalX. Curr Protoc Bioinformatics **Chapter 2:**Unit 2 3.

97. **Timmers, A. C., M. C. Auriac, and G. Truchet.** 1999. Refined analysis of early symbiotic steps of the *Rhizobium*-Medicago interaction in relationship with microtubular cytoskeleton rearrangements. Development **126:**3617-3628.

98. **Turner, L., W. S. Ryu, and H. C. Berg.** 2000. Real-time imaging of fluorescent flagellar filaments. J Bacteriol **182:**2793-2801.

99. **Vonderviszt, F., R. Ishima, K. Akasaka, and S. Aizawa.** 1992. Terminal disorder: a common structural feature of the axial proteins of bacterial flagellum? J Mol Biol **226:**575-579.

100. **Wagner, V.** 2006. Funktions- und Lokalisierungsanalyse des Chemotaxisproteins CheX von *Sinorhizobium meliloti* (Functional analysis and localization of the chemotaxis protein CheX from *Sinorhizobium meliloti*). Universität Regensburg, Regensburg.

101. **Welch, M., N. Chinardet, L. Mourey, C. Birck, and J. P. Samama.** 1998. Structure of the CheY-binding domain of histidine kinase CheA in complex with CheY. Nat Struct Biol **5:**25-29.

102. **Wilkins, M. R., E. Gasteiger, A. Bairoch, J. C. Sanchez, K. L. Williams, R. D. Appel, and D. F. Hochstrasser.** 1999. Protein identification and analysis tools in the ExPASy server. Methods Mol Biol **112:**531-552.

103. **Zhao, R., E. J. Collins, R. B. Bourret, and R. E. Silversmith.** 2002. Structure and catalytic mechanism of the *E. coli* chemotaxis phosphatase CheZ. Nat Struct Biol **9:**570-575.

Appendix. Amino acid sequence alignment of CheA from *S. meliloti* and *E. coli*. The domains are indicated above the alignment. The blue shaded region covers the P2 domain. Red residues indicate *S. meliloti* P2 domain amino acids in excess of the *E. coli* P2 domain. The CheS binding domain is indicated by a blue line below the alignment in P2, while the CheY2 binding domain is indicated by a green line. Histidine residues marked in blue indicate the conserved phosphotransfer sites on the P1 domain.

```
                                P1
                  ____________________________________________________
                 ....|....| ....|....| ....|....| ....|....| ....|....|
                          10         20         30         40         50
S. meli          --MDMNEIKE IFFQECEEQL AELESGLLKL NDG---DRDP ETVNAVFRAV
E. coli          MSMDISDFYQ TFFDEADELL ADMEQHLLVL QPE---APDA EQLNAIFRAA

                                P1
                  ____________________________________________________
                 ....|....| ....|....| ....|....| ....|....| ....|....|
                          60         70         80         90        100
S. meli          HSIKGGAGAF GLDDLVSFAH VFETTLDCVR SNRLEPNQDV LKVMLRSADV
E. coli          HSIKGGAGTF GFSVLQETTH LMENLLDEAR RGEMQLNTDI INLFLETKDI

                                P1                                 P2
                  ____________________________________  ____________
                 ....|....| ....|....| ....|....| ....|....| ....|....|
                         110        120        130        140        150
S. meli          LADLTNAARD GGGVDEARSR QLIKELEALA NG---ELP-- QAAA-----E
E. coli          MQEQLDAYKQ SQEPDAASFD YICQALRQLA LE-------- ----------

                                P2
                  ____________________________________________________
                 ....|....| ....|....| ....|....| ....|....| ....|....|
                         160        170        180        190        200
S. meli          SAPKTTPAGV APAAPVVNEE GFQPVAFSFD -DFETGDEP- TIEPSTYEIV
E. coli          ---------- AKGETPSAVT RLSVVAKSEP QDEQSRSQS- -----PRRII

                                P2
                  ____________________________________________________
                 ....|....| ....|....| ....|....| ....|....| ....|....|
                         210        220        230        240        250
S. meli          FKPKSDLYSK GNDATLLLRD LSRLGEMSIH CNMDTLPPLD RMNPEEAYFS
E. coli          LSR-----LK AGEVDLLEEE LGHLTTLTDV VKG-----AD SLS-------

                                P2
                  ____________________________________________________
                 ....|....| ....|....| ....|....| ....|....| ....|....|
                         260        270        280        290        300
S. meli          WKISLKTDKG EEAIRSVFEF AEWDCELDVA ---LAGGTVG MDEDLPMQPV
E. coli          --AILPGDIA EDDITAVLCF VIEADQITFE ---------- ----------

                                P2
                  ____________________________________________________
                 ....|....| ....|....| ....|....| ....|....| ....|....|
                         310        320        330        340        350
S. meli          PFDLSILEDE AQAP--AGEE DRAAASEGDS RNAAVAAAQT ASNVLQMAQS
E. coli          ---------- ---------- ---------- -TVEVSPKIS TPPVLKL---
```

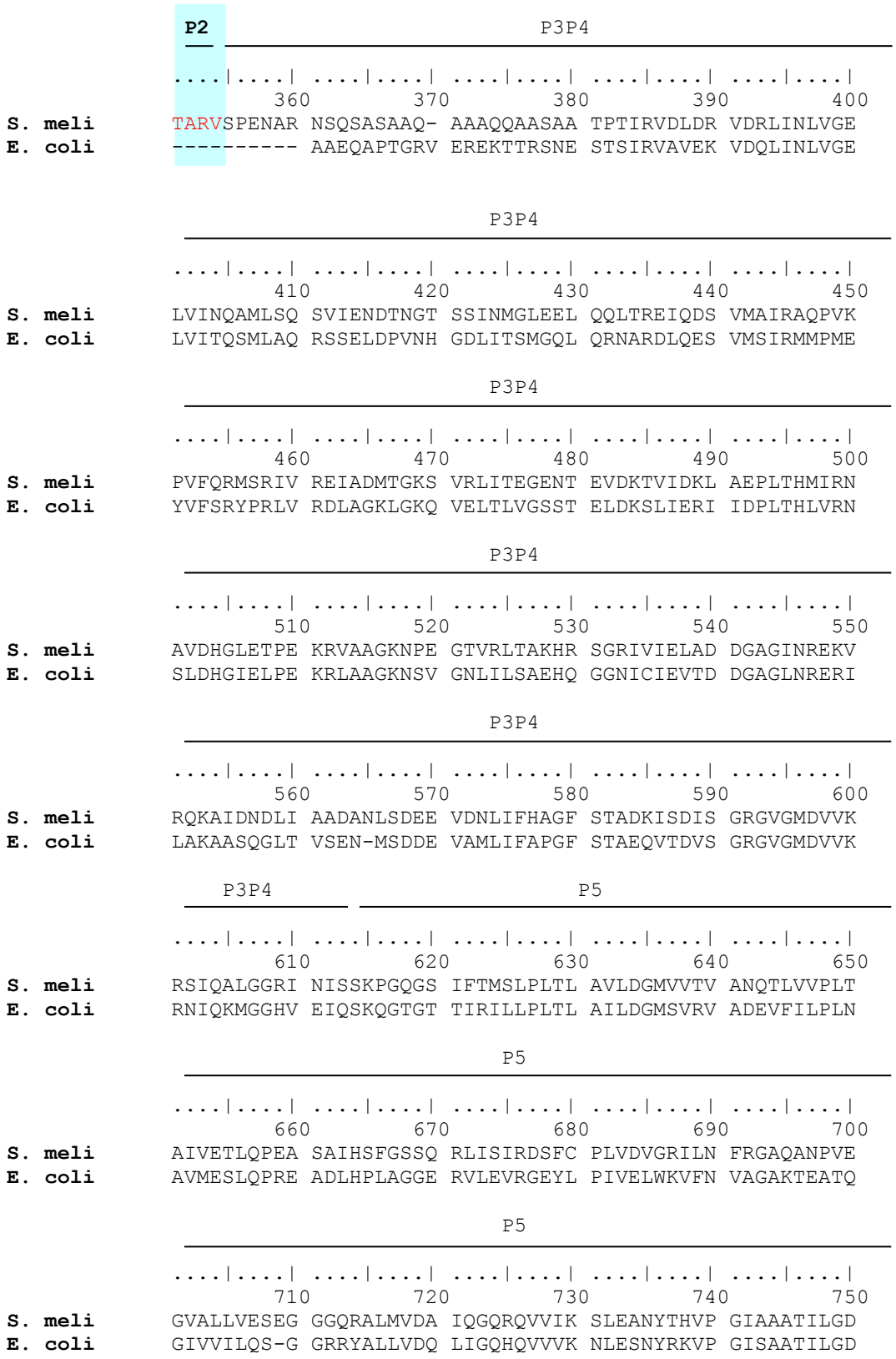
P2
P3P4
P3P4
P3P4
P3P4
P3P4
P5
P5
P5
360 370 380 390 400
S. meli TARVSPENAR NSQSASAAQ- AAAQQAASAA TPTIRVDLDR VDRLINLVGE
E. coli ---------- AAEQAPTGRV EREKTTRSNE STSIRVAVEK VDQLINLVGE
410 420 430 440 450
S. meli LVINQAMLSQ SVIENDTNGT SSINMGLEEL QQLTREIQDS VMAIRAQPVK
E. coli LVITQSMLAQ RSSELDPVNH GDLITSMGQL QRNARDLQES VMSIRMMPME
460 470 480 490 500
S. meli PVFQRMSRIV REIADMTGKS VRLITEGENT EVDKTVIDKL AEPLTHMIRN
E. coli YVFSRYPRLV RDLAGKLGKQ VELTLVGSST ELDKSLIERI IDPLTHLVRN
510 520 530 540 550
S. meli AVDHGLETPE KRVAAGKNPE GTVRLTAKHR SGRIVIELAD DGAGINREKV
E. coli SLDHGIELPE KRLAAGKNSV GNLILSAEHQ GGNICIEVTD DGAGLNRERI
560 570 580 590 600
S. meli RQKAIDNDLI AADANLSDEE VDNLIFHAGF STADKISDIS GRGVGMDVVK
E. coli LAKAASQGLT VSEN-MSDDE VAMLIFAPGF STAEQVTDVS GRGVGMDVVK
610 620 630 640 650
S. meli RSIQALGGRI NISSKPGQGS IFTMSLPLTL AVLDGMVVTV ANQTLVVPLT
E. coli RNIQKMGGHV EIQSKQGTGT TIRILLPLTL AILDGMSVRV ADEVFILPLN
660 670 680 690 700
S. meli AIVETLQPEA SAIHSFGSSQ RLISIRDSFC PLVDVGRILN FRGAQANPVE
E. coli AVMESLQPRE ADLHPLAGGE RVLEVRGEYL PIVELWKVFN VAGAKTEATQ
710 720 730 740 750
S. meli GVALLVESEG GGQRALMVDA IQGQRQVVIK SLEANYTHVP GIAAATILGD
E. coli GIVVILQS-G GRRYALLVDQ LIGQHQVVVK NLESNYRKVP GISAATILGD

```
                        P5
                  ____________________________________

                  ....|....| ....|....| ....|....| ....
                          760        770        780
S. meli           GRVALILDVD AIVAASR--- GQSLKPEMSL AAAG
E. coli           GSVALIVDVS ALQAINR--- ----EQRMAN TAA-
```